Hydrodynamic and interfacial patterns with broken space-time symmetry

Raymond E. Goldstein* and Gemunu H. Gunaratne†
The James Franck Institute and the Enrico Fermi Institute, The University of Chicago, 5640 Ellis Avenue, Chicago, Illinois 60637

L. Gil and P. Coullet
Laboratoire de Physique Théorique, Université de Nice, Nice CEDEX 06034, France
(Received 30 April 1990; revised manuscript received 10 December 1990)

In a variety of one-dimensional nonequilibrium systems, there exist uniform states that may undergo bifurcations to spatially periodic states. The long-wavelength dynamics of these spatial patterns, such as an array of convective rolls or a driven interface between two thermodynamic phases, can often be derived on the basis of the symmetries of the physical system. Secondary bifurcations of these patterns may be associated with the subsequent loss of remaining symmetries. Here, we study the transition that results from the loss of reflection symmetry (parity) and show that observations made in several recent experiments appear to be signatures of this bifurcation. Most of the common features seen in the disparate experiments follow from the simplest Ginzburg-Landau equations covariant under the remaining symmetries. It is shown that nucleated localized regions of broken parity travel in a direction determined by the sense of the asymmetry, and the passage of a localized inclusion of broken parity leads to a change in the wavelength of the underlying modulated state, and leaves the system closer to an invariant wavelength. Such behavior is in close correspondence with the properties of "solitary modes" seen in experiment. When a system supports extended regions of broken parity, a boundary between those of opposite parity can be considered as a source or sink of asymmetric cells and a "spatiotemporal grain boundary." The creation or destruction of cells at the interface is reminiscent of "phase slip centers" in one-dimensional superconductors. The simplest dynamics consistent with the symmetries are identical to those of the time-dependent Ginzburg-Landau equation for a superconductor in an applied electric field. The experimental observation of approximate length subtraction of colliding regions of broken parity follows from this analogy.

I. INTRODUCTION AND SUMMARY OF RESULTS

Close to the onset of many hydrodynamic transitions, the divergence of both length and time scales results in dynamics whose form transcends microscopic details. As a consequence, many general features of the large-scale evolution may be deduced from the underlying symmetries of the system. Consider as an example a solid-liquid interface translated at fixed velocity through a stationary temperature gradient G. As the velocity v is increased, the damping effects of interfacial tension cease to provide stability against diffusional effects that destabilize the interface. The ensuing transition, known as the Mullins-Sekerka[1] instability, occurs at a well-defined velocity $v_c(G)$. Prior to the transition, the interface $U_0(x,t)$ is stationary and planar, and hence is invariant under spatial and temporal translations,

$$x \to x+\Delta, \quad t \to t+\theta \ , \tag{1.1}$$

for arbitrary Δ and θ, as well as under reflections of time and space,

$$x \to -x, \quad t \to -t \ . \tag{1.2}$$

These invariances of the homogeneous pattern coincide with the full symmetry operations of space itself, and therefore, of course, with the underlying symmetries of the microscopic equations of motion.

Beyond the instability (i.e., for $v > v_c$), the interface pattern becomes "cellular" (periodic) and is invariant only under the more restricted translations,

$$x \to x+n\lambda, \quad t \to t+\theta \ , \tag{1.3}$$

where λ is the wavelength of the pattern, n is an integer, and again θ is arbitrary. However, the reflection symmetries (1.2) are retained. In general, only in the case of continuous transitions, and then only asymptotically close to the onset of the instability, does the pattern exhibit "up-down" ($U \to -U$) symmetry.

Here, we ask the question: What is the nature of secondary transitions that break one or more of the remaining invariances of cellular patterns? Interest in this issue stems from a variety of recent experiments[2–7] on one-dimensional pattern-forming systems that have provided evidence of rather universal behavior involving asymmetric distortions of periodic patterns. Thus motivated, we study here[8,9] in particular the dynamics of an instability at which the time-reversal symmetry and parity of the pattern are broken.

We begin in Sec. II with a brief summary of the varied experiments, highlighting those features most suggestive of the existence of a parity-breaking bifurcation. As in many hydrodynamic instabilities, the long-wavelength

slow evolution of the pattern may be reduced to that of a dynamical system with few degrees of freedom whose amplitudes serve as nonequilibrium order parameters. A mathematical description of patterns with broken parity entails an identification of the order parameter, and leads to important symmetry considerations that guide the formulation of model equations of motion. Such symmetry principles may be derived purely on the basis of the invariance of the dynamics to changes in the viewpoint of an observer,[8] and also by certain group-theoretical arguments.[10]

Section III is a detailed discussion of a simplified model of a parity-breaking transition, with particular emphasis on the subcritical (first-order) case (this variant appearing most relevant to the experiments on directional solidification). Within this model, we find a natural explanation for the properties of traveling regions of distorted cells (termed "solitary modes"[2] and "solitary tilt waves"[3] in the different experiments); they are nucleated inclusions of the broken-parity state. The proposed model takes the form of coupled Ginzburg-Landau equations for the amplitude of the broken parity and the phase of the pattern. As with all normal form expansions, the phenomenological parameters that appear in the dynamical laws are in principle derivable from the underlying nonlinear equations of motion for the pattern itself by means of a multiple time-scale analysis.[11] Owing to the complexity of the dynamics, stemming largely from the nonlinear boundary conditions and nonlocal effects in the various systems, we do not attempt that analysis here.[12]

Contrary to physical systems near equilibrium, for which the notion of a variational principle is valid, we expect nonvariational contributions to the dynamics in the systems under study here. The standard theory of kink dynamics is used to determine certain basic physical consequences of these and other terms. This is followed by a discussion of the mechanisms by which propagating nucleated inclusions of a broken-parity state act to alter and relax the wavelength of a pattern on which they travel. A brief discussion of related phenomena in the case of a supercritical bifurcation is also presented.

The simple model described and analyzed in Sec. III neglects certain important considerations that appear to play crucial roles in the dynamics of defect structures in patterns with broken parity. Section IV describes a phenomenological treatment of the coupling between the symmetric and antisymmetric components into which a pattern is resolved. A strong similarity is demonstrated between these dynamics and that of a superconductor in an applied electric field as described by the time-dependent Ginzburg-Landau model. The boundary between two regions of broken parity (space-time symmetry) is an example of a "spatiotemporal grain boundary" and finds a natural description in this model. Such a boundary is found also to resemble objects known as "phase slip oscillators" in one-dimensional superconductors. Certain issues related to these defects are first addressed in the context of a simplified *spatially forced* Ginzburg-Landau model, which is then generalized to be applicable to systems with broken parity.

A summary of the qualitative comparisons possible between theory and experiment is presented in Sec. V, along with a number of important areas that remain to be explored. Several explicit experiments are proposed as incisive tests of the hypothesis advanced herein. Possible future extensions of the present theoretical work are discussed in Sec. VI. Finally, Sec. VII concludes the present work with suggested directions for a more microscopic treatment of parity-breaking transitions. On the basis of certain common features in the various experimental systems, we advance a conjecture concerning the origin of the "universality" of this phenomenon.

II. PATTERNS WITH BROKEN PARITY

A. Examples

1. Directional solidification of liquid crystals

In studies[13] of the dynamics of the interface between nematic and isotropic phases of the liquid-crystal octylcyanobiphenyl (8CB) with small amounts of added impurities, it was found that there exists a primary transition whose properties are those of the Mullins-Sekerka (MS) instability. The association is based on the scaling of the onset velocity v_{MS} with the applied temperature gradient G, and the impurity concentration c, as well as features of the stability diagram. More recent studies[2,14] have shown the existence of so-called "solitary modes" far beyond the onset of the primary instability [Fig. 1(a)]. These traveling inclusions possess many interesting properties which we list below for future reference.

(a) There exists a second characteristic velocity $v_2(G)$ beyond which nucleated solitary modes propagate freely without decaying.

(b) The traveling domains are *typically* produced after a quench to a *higher* pulling speed. At the final velocity, the selected wavelength of the periodic pattern is smaller. Once formed, a domain smoothly disappears if the interface velocity is reduced sufficiently.

(c) The sense of asymmetry of the pattern within a solitary mode is precisely related to its direction of motion, and does not change during its propagation.

(d) The symmetric pattern left in the wake of a solitary mode generally has a shorter wavelength than the pattern into which the mode propagated, and this phenomenon is correlated with the spreading of the region of asymmetric cells.

(e) The wavelength of the asymmetric pattern is larger than that of the symmetric patterns bounding it.

(f) There exists no correlation between the wavelength change induced by the motion of a solitary mode and its mean lateral velocity. There is, however, an approximately linear relation between the lateral velocity and the velocity with which the pattern is translated through the temperature gradient.

(g) Successive passage of solitary modes appears to relax the wavelength of the pattern to a steady value.

(h) Two solitary modes of opposite sense of asymmetry, traveling in opposite directions, undergo collisions with an approximate rule of length subtraction; the remaining mode has a length approximately equal to the difference

in length between the original two, and travels in the direction of the longer one. See Fig. 1(b).

(i) During the course of a collision new symmetric cells are created in the collision region.

(j) Both sources and sinks of traveling waves have been observed.

2. *Directional solidification of eutectic mixtures*

In the related class of experiments[3] on directional solidification of eutectic mixtures of CBr_4 and C_2Cl_6, traveling regions of broken symmetry were discovered[15] which appear to be analogous to the solitary modes described above. The moving interface found in solidification of eutectic mixtures is significantly more complex than that found in a pure substance, for it is a locus of three-phase coexistence, involving a liquid mixture and two solid phases of differing composition. The latter are arranged in bands parallel to the direction of interface motion (i.e., normal to the mean interface), with *relative* widths given by the lever rule appropriate to the phase diagram below the eutectic point. The actual widths of the bands appear to be determined by a nonlinear wavelength selection mechanism.[16] This banded structure appears at arbitrarily small forward interface velocities. Unlike in the solidification of a one-component system, the history of lateral interface distortions is recorded in these bands. The observed traveling inclusions distort the lamellar structure so that it tilts from the interface normal, giving rise to the name "solitary tilt waves." The space-time portrait in Fig. 1(a) illustrates the meaning of this terminology in the case of directional solidification of liquid crystals. The most important properties of tilt waves are listed below.

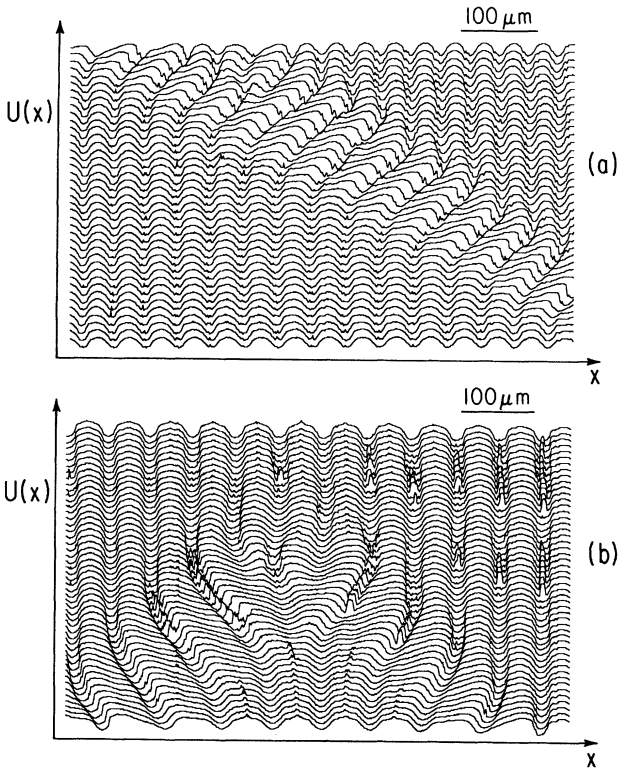

FIG. 1. Space-time portraits of "solitary-mode" motion across the interface between isotropic and nematic phases of a liquid crystal in a directional solidification experiment. (a) Motion of a single solitary mode, with time increasing upward. (b) Collision of two solitary modes and the creation of new cellular structures. Images in (a) and (b) are displayed at intervals of 1 and 0.4 sec, respectively. Courtesy of Simon, Flesselles, and Libchaber.

(a) Tilt waves are observed only beyond a characteristic interface velocity.

(b) The creation of tilt waves typically involves a quench to higher velocities, at which point the selected wavelength of the pattern is smaller than that at the initial velocity. Velocity quenches of the opposite sign do not produce tilt waves.

(c) The edges of tilt waves may be parallel, in which case the wavelengths of the patterns on its two sides are identical, or they may be skewed. In the latter case, a spreading width of the tilt wave is associated with a wavelength decrease in the pattern left behind. Inside the tilt wave, the wavelength of the basic lamellar pattern is larger than that of the untilted regions on either side.

(d) Collisions between tilt waves moving in opposite directions roughly obey a law of length subtraction, much like that found in the liquid-crystal solidification experiments.

3. *Directional viscous fingering*

Recent studies[4] of the meniscus between a fluid entrained between two internally tangent cylinders have revealed a complex dynamics in many ways similar to that of an advancing solid-liquid interface. Progressive increase of the rotational speed of one of the cylinders, say, the inner, with the outer cylinder fixed, leads to a destabilization of the planar meniscus, producing a cellular pattern much like that seen in the Mullins-Sekerka instability. Counterrotation of the outer cylinder at sufficient velocity then leads to a traveling-wave state. Below is a summary of the important observations concerning these states.

(a) The phase velocity of the traveling-wave state varies as the square root of the deviation of the control parameter from its value at onset.

(b) The typical traveling-wave pattern formed by rotation of the outer cylinder consists of one or more "defects" that take the form of sources or sinks of traveling waves, being the junction between two domains or opposite wave propagation direction.

(c) In the regime of traveling domains, collisions may result in either partial or total annihilation.

4. *Rayleigh-Bénard convection*

Experiments on Rayleigh-Bénard convection in narrow rectangular channels have revealed the existence of traveling abnormal convective cells far beyond the critical Rayleigh number for the onset of convection.[5] The important characteristics of these moving structures are as

follows.

(a) The distorted cells are significantly longer than the static convective cells.

(b) Abnormal cells may travel in either direction across the basic pattern.

(c) A collision between two counterpropagating stretched cells results in a long-lived pair, the center of which eventually is the site of the creation of new convective cells.

5. *Parametric excitation of waves*

Studies of the parametric excitation of waves on the surface of water contained an annular cell[7] have revealed that the well-known standing-wave pattern that occurs at small excitation amplitude may undergo secondary instabilities involving propagative phase dynamics. That is, beyond a characteristic driving force the entire pattern may begin to "drift" at a constant speed. This instability is preceded by an oscillatory phase behavior corresponding to a compression mode.

B. Hypothesis: A new transition

The fundamental hypothesis advanced here is the following: The experimentally observed asymmetric cellular structures are inclusions of a dynamical state with broken parity. With this viewpoint, the commonality of the behavior of the diverse experimental systems described above follows as a consequence of the separation of spatial and temporal scales between the cellular pattern and the degrees of freedom characterizing the broken parity. It is further conjectured that in a state with a uniformly asymmetric pattern in space, we may employ the usual decomposition of an asymmetric function into a sum of symmetric and antisymmetric functions. In the simplest description, we ignore the degrees of freedom associated with the symmetric component of the pattern, and write for the spatial pattern U the decomposition

$$U(x,t)=U_S(x+\phi(x,t))+A(x,t)U_A(x+\phi(x,t)) , \tag{2.1}$$

where the envelope function $A(x,t)$ serves as the order parameter of the broken parity. The parity-breaking transition is then seen as an exchange of stability between symmetric states, with $A=0$, and asymmetric states, with $A\neq 0$.

The decomposition in (2.1) allows us to describe the observed patterns in a very simple way, as shown in Fig. 2. A localized region of distorted cellular structures is a "bubble" or "inclusion" of the state with nonzero A. The two possible signs of A [middle of Figs. 2(a) and 2(b)] correspond to the two observed senses of the asymmetry. To complete the qualitative description of asymmetric patterns in the context of Eq. (2.1), note that a linear phase function $\phi=Qx$ describes a pattern with an altered wave vector,

$$q=q_0(1+Q), \tag{2.2}$$

The bottoms of Figs. 2(a) and 2(b) show that the phase function associated with a locally distorted region is essentially bilinear. The positive phase gradient to the left of the region of asymmetric cells (a), and to the right in (b), creates a pattern with a higher wave vector (shorter wavelength), whereas the negative phase gradient within the distorted cells leads to a longer wavelength, as

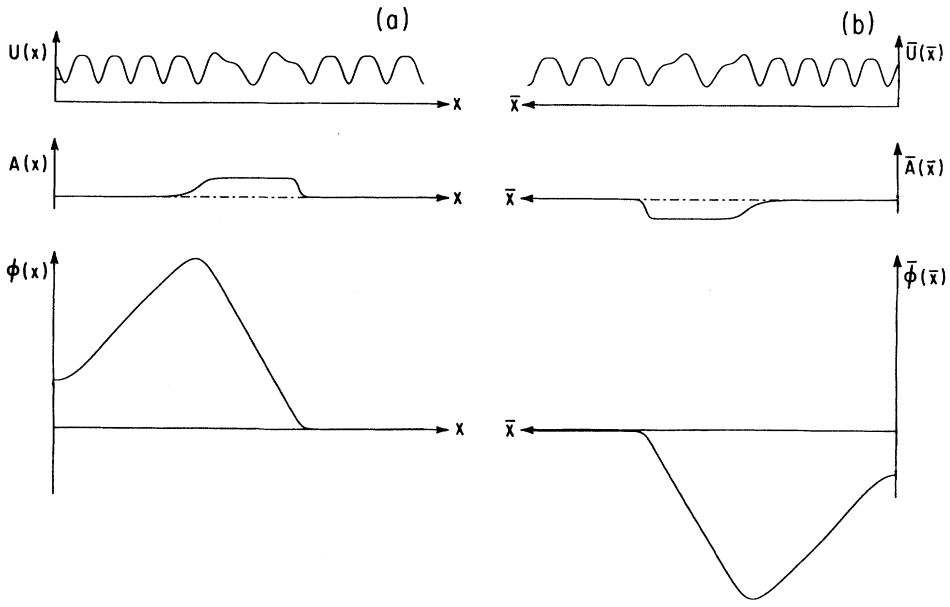

FIG. 2. Resolution of the one-dimensional pattern into symmetric and antisymmetric components. Two modulated patterns with "solitary modes" of opposite sense are shown in (a) and (b), and are related by the transformations in Eqs. (2.4)–(2.6). These patterns are described by broken-parity amplitudes $A(x)$ and associated phase functions $\phi(x)$ shown below each. The patterns in (a) and (b) are obtained from A and ϕ through Eq. (2.1)

seen in experiment. In this form, the motion of the distorted cells coincides both with the propagation of the bubble of asymmetry amplitude and with the advancing "front" of negative phase gradient. We shall see below that the motion of the inclusion is reduced to that of its two edges.

As in all such approaches based on amplitude equations, it is supposed that the spatial variations of A and ϕ are on length scales long compared to the wavelength of the cellular pattern itself, and it is only then that the notion of symmetric and antisymmetric components is absolutely well defined. From the experimental point of view this criterion is only marginally valid, precluding us from making quantitative statements. Nevertheless, the essential symmetry considerations remain valid.

In addition to the assumed unstable mode A, we have indicated that the phase ϕ of the pattern is a dynamical variable, in recognition of the fact that a periodic structure always has a marginally unstable mode arising from its translational invariance in space. The dynamics of A will in general be coupled to this phase mode.[8,10] In this description, note that there is only a single phase function associated with the two components, since their relative parity symmetry would not otherwise be clearly defined.[17]

We emphasize that the description advanced here is *not* a theory of the symmetric and antisymmetric functions U_S and U_A. A determination of these requires microscopic calculations that incorporate the particular nonlinear physics associated with each system. It is by focusing on the envelope function and the phase that we may address the full extent of universality in the dynamics of broken parity.

In the bulk of what follows we shall cast the discussion in a language appropriate to directional solidification of a one-component system. Analysis of the interface patterns has shown that reasonable forms for the symmetric and antisymmetric functions are

$$U_S(z)\simeq a_1\cos(q_0 z)+b_1\cos(2q_0 z)\ , \tag{2.3a}$$

$$U_A(z)\simeq c_1\sin(q_0 z)+d_1\sin(2q_0 z)\ , \tag{2.3b}$$

the relative amplitudes a_1, etc., being deduced from experiment. In subsequent calculations, reconstructed interface patterns will be based on (2.3).

The resolution given by Eqs. (2.1) and (2.3) immediately explains two important observations noted in the experiments. First, the physical shape of the individual asymmetric cells does not change in time, unlike that due to the passage of the familiar solitons.[18] Second, the internal structure of distorted cells, with two unequal maxima, follows directly from the presence of the antisymmetric second harmonic $\sin(2q_0 z)$.

C. Symmetry considerations

The symmetries of the equations of motion may be deduced from the invariance of the dynamics seen by observers on opposite sides of the plane of the pattern. Let $U(x)$ and $\bar{U}(\bar{x})$ be the interface as seen by the two, as shown in Fig. 2. The lateral coordinates of the viewers are clearly related by

$$\bar{x}=-x\ , \tag{2.4}$$

so a shift $\phi(x)$ for one corresponds to $-\bar{\phi}(\bar{x})$ for the other. The vertical displacements seen by the two must be identical, and hence (with the antisymmetry of U_A), the amplitudes must be related by $\bar{A}(\bar{x})=-A(x)$. Thus, we require the covariances

$$\bar{A}(-x)=-A(x),\quad \bar{\phi}(-x)=-\phi(x) \tag{2.5}$$

for all time t, and hence

$$\bar{A}_t(-x)=-A_t(x),\quad \bar{\phi}_t(-x)=-\phi_t(x)\ . \tag{2.6}$$

The highly dissipative dynamics seen experimentally suggests relaxational equations of motion of the form

$$\begin{aligned} A_t&=\mathcal{R}_A(A,A_x,A_{xx},\ldots,\phi_x,\phi_{xx},\ldots)\ ,\\ \phi_t&=\mathcal{R}_\phi(A,A_x,A_{xx},\ldots,\phi_x,\phi_{xx},\ldots)\ , \end{aligned} \tag{2.7}$$

where the nonlinear operators $\mathcal{R}_A$ and $\mathcal{R}_\phi$ are *odd* under the transformations $x\to -x$, $A\to -A$, and $\phi\to -\phi$. Observe further that the invariance of the dynamics to the absolute value of the phase of the pattern implies that the $\mathcal{R}_A,\mathcal{R}_\phi$ in (2.7) may depend on ϕ only through its gradients.

III. MODEL DYNAMICS

A. Equations of motion

There exists no known variational principle by which the dynamics of nonequilibrium pattern formation may be deduced, so we do not expect the equations of motion for the phase and amplitude to be derivable from a Lyapunov function. Nevertheless, we propose that the essential aspects of the dynamics at a parity-breaking bifurcation may be understood by separating the evolution of A and ϕ into "variational" and "nonvariational" parts. The former is derived from the relation

$$A_t=-\delta\mathcal{F}_A/\delta A\ , \tag{3.1}$$

with $\mathcal{F}_A$ the Lyapunov functional for the amplitude. In the spirit of an amplitude-equation approach, we shall postulate a model for $\mathcal{F}_A$ under the assumption that A and its gradients are small. The canonical form for this variational contribution is[19]

$$\mathcal{F}_A=\int dx\,(\tfrac{1}{2}A_x^2+F(A)+\cdots)\ , \tag{3.2}$$

yielding $A_t=A_{xx}-(\partial F/\partial A)$. The even polynomials $F(A)$,

$$F_1(A)=-\tfrac{1}{2}\mu A^2-\tfrac{1}{4}\alpha A^4+\tfrac{1}{6}A^6 \tag{3.3a}$$

and

$$F_2(A)=-\tfrac{1}{2}\mu A^2+\tfrac{1}{4}A^4\ , \tag{3.3b}$$

with $\alpha>0$, distinguish, respectively, between sub- and supercritical bifurcations. Note that in either case the two states represented by $\pm A^*$ are of equal stability, as required by symmetry. In the present interpretation, the motion of the region of broken parity reduces to that of

the two edges of the bubble. For supercritical parity-breaking bifurcations, such a kink propagates from an *unstable* state to a stable state, whereas for subcritical transitions the kink connects a *metastable* state to a stable one.

As is typically the case in Ginzburg-Landau approaches, we shall assume in most discussions that the important variation of the parameters μ and α with the experimental control parameter r is contained in μ. Specializing to the subcritical case, Fig. 3(a) illustrates the qualitatively different forms taken by F_1 with μ. Within a small region centered around μ^*, the "Maxwell point," the competing symmetric and broken-parity states are both linearly stable, their relative stability changing at μ^*. For $\mu > 0$ the symmetric state is linearly unstable.

The variational contributions described by (3.1), (3.2), and (3.3) are clearly consistent with the symmetries required of the parity-breaking dynamics, but do not, for instance, include terms odd under the transformation $x \rightarrow -x$. For the purpose of understanding the forces that affect the edges of a bubble, all further additive nonlinear terms in the amplitude equations may be classified into two primary categories. Our focus here will be on the qualitative consequences of these kinds of nonlinearities, and therefore we shall investigate only the lowest-order terms of these groups; a more detailed study of the entire panology of nonlinearities is deferred. The simplified equation of motion adopted here for A is

$$A_t = A_{xx} - \frac{\partial F}{\partial A} + \gamma A A_x + \epsilon A \phi_x + \cdots , \tag{3.4}$$

where γ and ϵ are phenomenological parameters whose signs are as yet unspecified. Below, it is shown that the terms with the symmetry of $A A_x$ are primarily responsible for the translation of the center of mass of inclusions of the state with nonzero A, while terms like $\epsilon A \phi_x$, which depend on the phase gradient, play an important role in wavelength relaxation. Within the context of subcritical parity-breaking bifurcations and the description of solitary modes as droplets of the traveling-wave state, all other nonlinearities that are allowed by symmetry in Eq. (3.4), such as ϕ_{xx}, etc., may be classified into a few distinct groups on the basis of their effects on the motion of those bubbles. For this reason, we focus on terms that epitomize the behavior of these few groups. In the supercritical case, certain new terms may produce qualitatively different behavior.[20]

In the simplest case, the appropriate functional for the phase tends to drive the system to the underlying wave vector q_0, and is quadratic in the gradients

$$\mathcal{F}_\phi = \int dx (\phi_x^2 + \cdots) , \tag{3.5}$$

yielding the diffusive form $\phi_t = \phi_{xx}$. Below we show that much of the phenomena of wavelength selection and the dynamics of defects arises from the lowest-order coupling between the phase dynamics and A, embodied in the phase equation

$$\phi_t = \phi_{xx} + \omega A + \cdots , \tag{3.6}$$

with ω also of as yet unspecified sign. Thus, a pattern with uniformly broken parity (i.e., nonzero A) has a phase that increases in magnitude linearly in time, and with the phase of the pattern entering as in Eq. (2.1), this yields a traveling-wave state. While the underlying dissipative dynamics of the pattern are, of course, not time-reversal invariant, we may classify the symmetries, including that of time-reversal invariance, of *steady-state, homogeneous* patterns. In this restricted sense of examining patterns before and after the bifurcation, we may say that the loss of reflection symmetry is coincident with the loss of time-reversed invariance. Again, it should be remarked that the dynamics proposed above explicitly neglect linear gradient terms such as A_{xx} in (3.6), and under certain circumstances[17] such cross terms may lead to qualitatively different behavior than implied by dynamics lacking them.

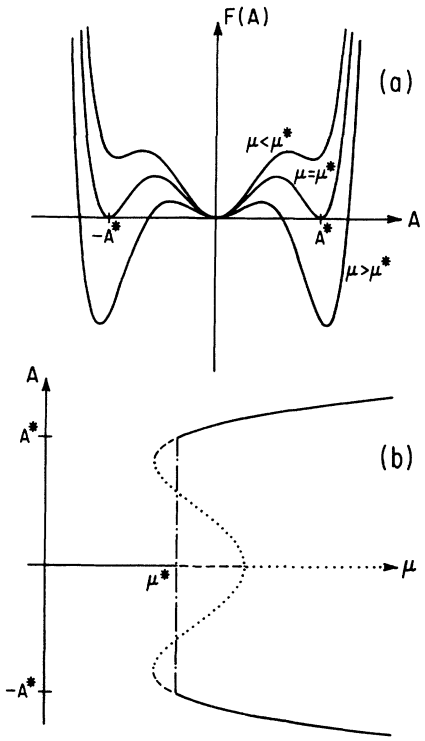

FIG. 3. (a) Lyapunov function appropriate to a subcritical bifurcation, at various values of the control parameter μ. (b) The stable (solid lines), metastable (dashed), and unstable (dotted) equilibrium values of the broken-parity order parameter as a function of μ. The vertical dash-dotted line at μ^* indicates the Maxwell point.

B. Subcritical bifurcations

1. Elementary dynamical considerations

We first investigate the linear stability of the basic pattern U_S toward antisymmetric perturbations. While for subcritical bifurcations the *nonlinear* stability of the pattern is perhaps most relevant to the creation of domains

of broken parity, an important qualitative principle is illustrated by considering first the linear stability. The relevant time-independent solutions to the dynamical equations for A and ϕ are

$$A_0=0, \quad \phi_0=p+Qx \ , \tag{3.7}$$

p being an arbitrary additive constant, with the linear term Qx in ϕ corresponding to a symmetric pattern with an altered wavelength. Writing

$$A=A_0+A', \quad \phi=\phi_0+\phi' \ , \tag{3.8}$$

we find to linear order

$$\partial_t \begin{bmatrix} A' \\ \phi' \end{bmatrix} = \begin{bmatrix} \partial_{xx}+\mu+\epsilon Q & 0 \\ \omega & \partial_{xx} \end{bmatrix} \begin{bmatrix} A' \\ \phi' \end{bmatrix} . \tag{3.9}$$

Assuming

$$(A',\phi') \sim \exp(\sigma t+ikx) \ ,$$

we obtain the dispersion relations for two eigenmodes e_1 and e_2, one a purely diffusive *phase mode,*

$$e_1 \propto \begin{bmatrix} 0 \\ 1 \end{bmatrix}, \quad \sigma_1=-k^2 \ , \tag{3.10}$$

the other a *mixed phase and amplitude mode,*

$$e_2 \propto \begin{bmatrix} \mu+\epsilon Q \\ \omega \end{bmatrix}, \quad \sigma_2=\mu+\epsilon Q-k^2 \ . \tag{3.11}$$

From (3.11) we may deduce the stability diagram shown in Fig. 4 for the case $\epsilon<0$, illustrating that the broken-parity transition may occur either by changes in the control parameter μ or by creation of a phase gradient with the appropriate sign. That is, when the pattern is stretched and $\epsilon<0$, or when the pattern is shrunk and $\epsilon>0$, the relative stability of the state at a given μ is reduced. As may be deduced from the potential in Fig. 3 and Eq. (3.3), the instability at $\mu=0$ corresponds to the transformation of the point $A=0$ from a metastable minimum to a local maximum of F. Before that value of μ, the pattern is *nonlinearly* unstable, and the above considerations have important consequences for the nucleation of inclusions of the broken-parity state (see Sec. III B 3).

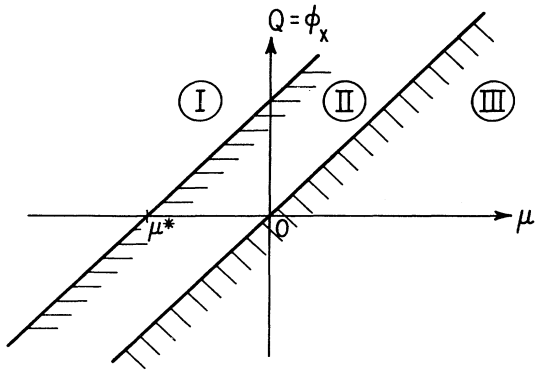

FIG. 4. Stability diagram for the basic pattern in the space of control parameter μ and phase gradient $Q \equiv \phi_x$, for $\epsilon<0$. The systems in regions I, II, and III are, respectively, absolutely stable, nonlinearly unstable, and linearly unstable to parity-breaking perturbations.

2. *Kink dynamics*

The hypothesis that the experimentally observed traveling cellular distortions in the various hydrodynamic patterns are inclusions of an antisymmetric state implies certain relationships between the characteristics of the envelope function bounding the inclusion and its direction of motion. To establish these, we begin by rewriting the amplitude equation for A as

$$A_t=A_{xx}+\mu^* A+\alpha A^3-A^5+\Delta\mu A+\gamma A A_x+\epsilon A\phi_x \ , \tag{3.12}$$

where

$$\Delta\mu \equiv \mu-\mu^* \tag{3.13}$$

is the deviation from the coexistence point. This form emphasizes the three kinds of forcing, associated with amplitudes $\Delta\mu$, γ, and ϵ, on the elementary kinks connecting states with $A=0$ and $A\neq 0$.

Recall first that there are four elementary kinks connecting the symmetric state $A=0$ with a broken symmetry state $A=\pm A^*$, as shown in Fig. 5. At the coexistence point $\mu=\mu^*=-\frac{3}{16}\alpha^2$, all four are of equal stability and subject to no forcing when in isolation. We adopt the labeling conventions shown in the figure, and refer to their *parity* (i.e., sign) and *orientation* (i.e., handedness). Let us solve for, say, $A_L^+(x)$. The other kinks may be obtained by a coordinate transformation and/or inversion. From Eq. (3.3), we have

$$0=\frac{d^2}{dx^2}A_L^+ +\mu^* A_L^+ +\alpha(A_L^+)^3-(A_L^+)^5 \ , \tag{3.14}$$

with the boundary conditions $A_L^+(-\infty)=0$ and $A_L^+(\infty)=A^*$. The ordinary differential equation (3.14)

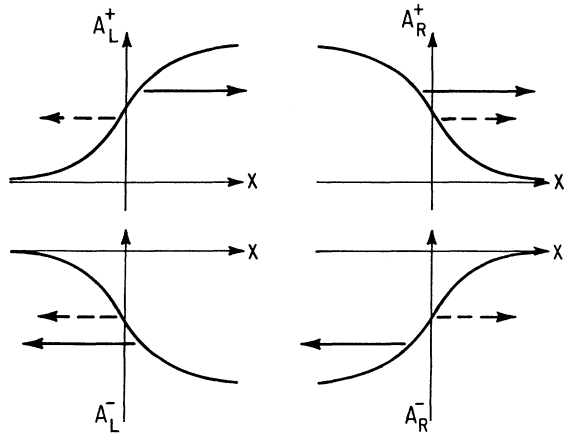

FIG. 5. Elementary kink structures and the forces acting on them. The dashed arrows give the direction of motion when $\mu>\mu^*$, while solid arrows indicate the effects of the term $\gamma A A_x$ for $\gamma<0$.

with these boundary conditions has the first integral

$$\frac{1}{2}\left[\frac{dA_L^+}{dx}\right]^2 = F_1(A_L^+) . \tag{3.15}$$

Integrating by partial fractions, and setting $A(x=0)=A^*/2$ for convenience, we obtain

$$A_L^+(x)=\frac{A^*}{[1+3\exp(-2x/\xi)]^{1/2}} , \tag{3.16}$$

where $A^*=\sqrt{3\alpha}/2$, and with the correlation length

$$\xi=\frac{\sqrt{3}}{A^{*2}}=\frac{4}{\sqrt{3}\alpha} . \tag{3.17}$$

The remaining kinks are then

$$\begin{aligned} A_R^+(x)&=A_L^+(-x) , \\ A_L^-(x)&=-A_L^+(x) , \\ A_R^-(x)&=-A_L^+(-x) . \end{aligned} \tag{3.18}$$

(a) Forcing induced by $\Delta\mu A$. Consider now the motion of these elementary kinks induced by a small deviation $\Delta\mu$ of the control parameter, its value at the Maxwell point, with $\Delta\mu>0$ stabilizing the states with $A\neq 0$ relative to the symmetric state, and vice versa. For widely separated kinks and for small forcing, the steady-state solution to the equation of motion is approximated by a traveling version of the kinks A_K plus a small correction of order $\Delta\mu$,[21,22]

$$A(x,t)\simeq A_L^+(z)+w_L^+(z), \quad z=x-x_L^+(t) \tag{3.19}$$

where $x_L^+(l)$ is the as yet unknown moving origin of the kink and w_L^+ is the as yet unknown correction. Substituting into the equations of motion, we obtain to leading order in w_L^+,

$$-\dot{x}_L^+\frac{d}{dz}A_L^+(z)=\mathcal{N}_{\mu^*}(A_L^+)+\Delta\mu\frac{\partial\mathcal{N}_{\mu^*}}{\partial\mu}(A_L^+) + \frac{\partial\mathcal{N}_{\mu^*}}{\partial A}(A_L^+)w_L^+ + \cdots , \tag{3.20}$$

dropping terms of order $(w_L^+)^2$, $w_L^+\dot{x}_L^+$, etc. Here,

$$\frac{\partial\mathcal{N}_{\mu^*}}{\partial\mu}(A_L^+)=A_L^+(z) \tag{3.21}$$

and

$$\frac{\partial\mathcal{N}_{\mu^*}}{\partial A}(A_L^+)=\frac{d^2}{dz^2}+\mu^*+3\alpha(A_L^+)^2-5(A_L^+)^4 . \tag{3.22}$$

Equation (3.22) may be cast in the form of a linear inhomogeneous ordinary differential equation for the correction w_L^+,

$$\mathcal{L}_L^+\left[z,\frac{d^2}{dz^2}\right]w_L^+=-\Delta\mu A_L^+(z)-\dot{x}_L^+\frac{d}{dz}A_L^+(z) , \tag{3.23}$$

where

$$\mathcal{L}_L^+=\frac{\partial\mathcal{N}_{\mu^*}}{\partial A}(A_L^+) . \tag{3.24}$$

Now, the existence of a first integral of the equations of motion guarantees that A is bounded in magnitude for all time, so we must eliminate any secular terms that would arise in inverting (3.23) to find w_L^+. The elimination of these terms is accomplished by choosing the velocity $\dot{x}_L^+$ in order that the right-hand side of (3.23) is orthogonal to the null space of the linear operator $\mathcal{L}_L^+$. Using the defining equation for the equilibrium kink

$$\mathcal{N}_{\mu^*}(A_L^+)=0 , \tag{3.25}$$

we differentiate to obtain

$$\frac{d}{dz}\mathcal{N}_{\mu^*}(A_L^+)=\frac{\partial\mathcal{N}_{\mu^*}}{\partial A}\frac{dA_L^+}{dz}\equiv\mathcal{L}\frac{dA_L^+}{dz}=0 . \tag{3.26}$$

Thus (dA_L^+/dz) is the eigenfunction of $\mathcal{L}_L^+$ with zero eigenvalue and hence is in its null space. Note that $\mathcal{L}_L^+$ is a self-adjoint operator. Orthogonalization means

$$0=\int dz\frac{dA_L^+(z)}{dz}\left[-\Delta\mu A_L^+(z)-\dot{x}_L^+\frac{dA_L^+(z)}{dz}\right] \tag{3.27}$$

or

$$\dot{x}_L^+=-\Delta\mu\frac{\int dz\, A_L^+(dA_L^+/dz)}{\int dz(dA_L^+/dz)^2} . \tag{3.28}$$

As is clear from the form (3.28), the velocity arising from deviations $\Delta\mu$ of the control parameters is (a) *even* under parity inversion (i.e., $A\rightarrow -A$) and (b) *odd* under reversal of the kink orientation [i.e., $A(z)\rightarrow A(-z)$], as shown in Fig. 5. With the closed form for the A_K, we obtain explicitly the velocities $\dot{x}_L^+$, etc., in terms of the parameters of the amplitude equation

$$\dot{x}_L^+(\Delta\mu)=-\frac{8}{\sqrt{3}\alpha}\Delta\mu . \tag{3.29}$$

Returning to the transformations connecting the kinks A_R^+, etc., to the basic kink A_L^+, we obtain

$$\begin{aligned} \dot{x}_R^+(\Delta\mu)&=-\dot{x}_L^+(\Delta\mu), \\ \dot{x}_L^-(\Delta\mu)&=\dot{x}_L^+(\Delta\mu) , \\ \dot{x}_R^-(\Delta\mu)&=\dot{x}_L^+(\Delta\mu) . \end{aligned} \tag{3.30}$$

(b) Forcing induced by $\gamma A A_x$ and $\epsilon A\phi_x$. The parity and orientational symmetries of the velocity induced by deviations from the coexistence point μ^* are to be contrasted with those arising from the coupling term $\gamma A A_x$ in the dynamics (3.3). Applying the kink-dynamics procedure as above, we obtain the velocity

$$\dot{x}_L^+(\gamma)=-\gamma\frac{\int dz\, A_L^+(dA_L^+/dz)^2}{\int dz\,(dA_L^+/dz)^2} , \tag{3.31}$$

which is antisymmetric under parity reversal and symmetric under orientational reversal, i.e.,

$$\dot{x}_R^+(\gamma)=\dot{x}_L^+(\gamma)\ ,$$
$$\dot{x}_L^-(\gamma)=-\dot{x}_L^+(\gamma), \tag{3.32}$$
$$\dot{x}_R^-(\gamma)=-\dot{x}_L^+(\gamma)\ ,$$

as shown by the dashed arrows in Fig. 5. Equation (3.31) may be simplified to

$$\dot{x}_L^+(\gamma)=-\frac{4\sqrt{3\alpha}}{15}\gamma\ . \tag{3.33}$$

The dynamic coupling of the phase gradient to the amplitude A is somewhat complicated by the rather nonlocal relation between the phase and amplitude implied by the phase dynamics $\phi_t=\phi_{xx}+\omega A$. Observe, however, that the *symmetries* of the associated forces on kinks in A may be deduced quite simply by viewing the phase dynamics as an inhomogeneous diffusion equation. That is, we rewrite (3.6) as

$$(\partial_t-\partial_{xx})\phi(x,t)=\omega A(x,t)$$

and then solve it formally as

$$\phi(x,t)=-\omega\int_{-\infty}^{\infty}dx'\int_{-\infty}^{\infty}dt'G(x,t;x',t')A(x',t')\ , \tag{3.34}$$

where G is the diffusional Green's function. From this, we see that the coupling $A\phi_x$ has the same symmetries under parity and orientational reversal as the term AA_x.

3. *Nucleated propagating inclusions*

With the view that traveling domains of asymmetric stretched cells are bubbles of the broken-parity state, we may understand the motion of those bubbles from the viewpoint that they are two kinks of opposite orientation joined together. From the analysis above it is clear that the velocities of the two edges of such a bubble are not equal; the mean velocity is controlled by the terms AA_x and $A\phi_x$, while the spreading rate (the difference in velocities) is controlled by the forcing $\Delta\mu A$ due to the deviation from the Maxwell point. Since the bifurcation is subcritical, a perturbation to the interface will only lead to a propagating inclusion if it is larger than the critical nucleus. The critical nucleus itself has a size that may be determined from a straightforward generalization of the kink-dynamics approach used in Sec. III B 2 (b).[23] For the dynamics of A alone, the size l_c of the critical nucleus scales with μ beyond the Maxwell point as $l_c\sim-\ln(\mu-\mu^*)$. In the present context, with the effective control parameter varying with the phase gradient, we see that the size of the critical nucleus scales as

$$l_c\sim-\ln(\mu+\epsilon\phi_x-\mu^*)\ .$$

Thus, nucleation of broken-parity inclusions is facilitated (in the sense of requiring a smaller critical nucleus) in altered symmetric patterns with $\epsilon\phi_x>0$.

Figure 6(a) shows the space-time evolution of a nucleated bubble for the parameter values $\mu=-0.15$, $\alpha=1.0$, $\epsilon=-1.0$, $\gamma=-2.0$, and $\omega=1.0$, obtained by numerical integration of the equations of motion.[24] After a short transient, the two edges of the bubble move with uniform, although unequal, velocities, leading to a linear spreading rate. As expected, we find that opposite-parity bubbles move in opposite directions with velocities and spreading rates of equal magnitude, and that the rate of spreading increases with $\mu-\mu^*$. In general, there is a second, qualitatively different regime of behavior in which the edges of an inclusion move in *opposite* directions, with velocities of different magnitude. This occurs when the forcing from the control parameter dominates the "advection" due to terms like AA_x and $A\phi_x$ in the dynamics.

The phase function ϕ associated with the amplitude in Fig. 6(a) is shown in Fig. 6(b). It exhibits an essentially bilinear form with a positive phase gradient left in the wake of the bubble and a negative phase gradient within the bubble itself. When A and ϕ are used to reconstruct the interface pattern (Fig. 7), we see many of the features of the experimental patterns (e.g., as in Fig. 1). First, the sense of asymmetry within a moving domain is preserved during its motion; there is no "flipping" of the asymmetry. Second, the wavelength of distorted cells is larger than those on either side when the pattern left behind has a shorter wavelength (see also Sec. IV). This results from the negative phase gradient within the bubble. Third, the nonzero phase velocity within the asymmetric regions

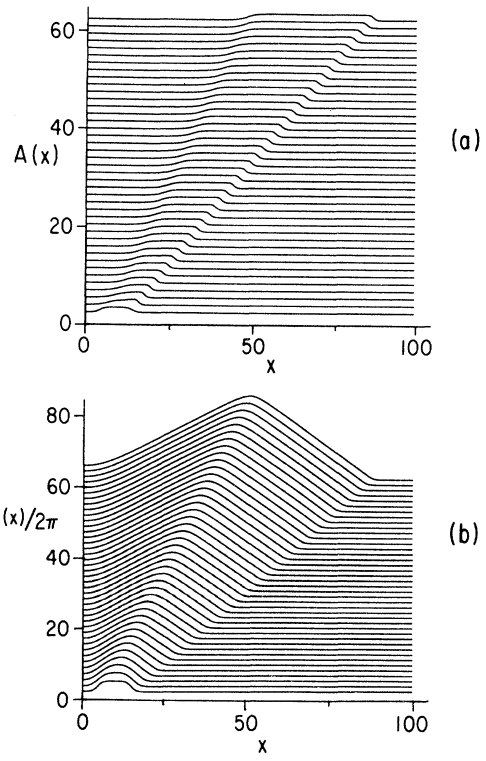

FIG. 6. Amplitude and phase of a propagating inclusion of broken parity, with time increasing upward and successive graphs offset for clarity. The bubble of nonzero order parameter A in (a) spreads uniformly as it moves, leaving behind a phase function (b) that is linear in x.

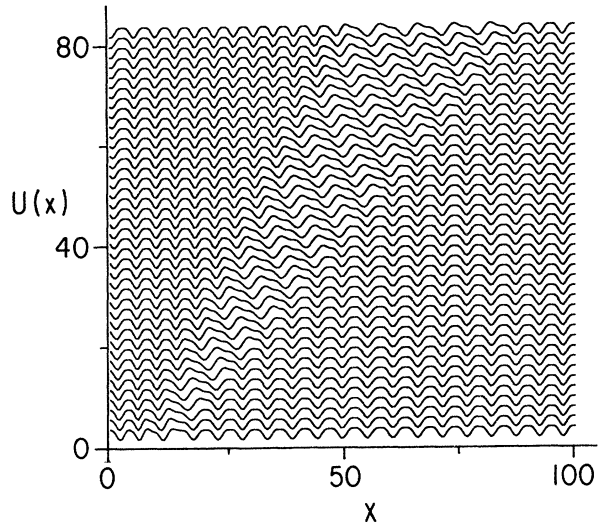

FIG. 7. Reconstructed interface pattern corresponding to the inclusion of broken parity in Fig. 6, using Eqs. (2.1) and (2.3).

leads to a space-time pattern in which the motion of an inclusion corresponds to a "tilt wave."

The phase gradient left in the wake of a solitary mode has important consequences for the behavior of subsequent traveling domains that pass through the same region. In Fig. 8 we plot the envelope function A over a period of time during which bubbles of broken parity were injected periodically at a fixed point in space. Observe that the spreading rate of a given bubble is smaller than that of the preceding one. Analysis of the phase of the pattern reveals also that the *difference* in wave-vector shift between the two sides of the parity bubble also steadily decreases; that is, the wavelength of the pattern relaxes to a fixed value. To understand this phenomenon, qualitatively like that seen in experiment, requires that we understand in detail the mechanism by which wavelengths are altered by solitary modes, a subject to which we now turn.

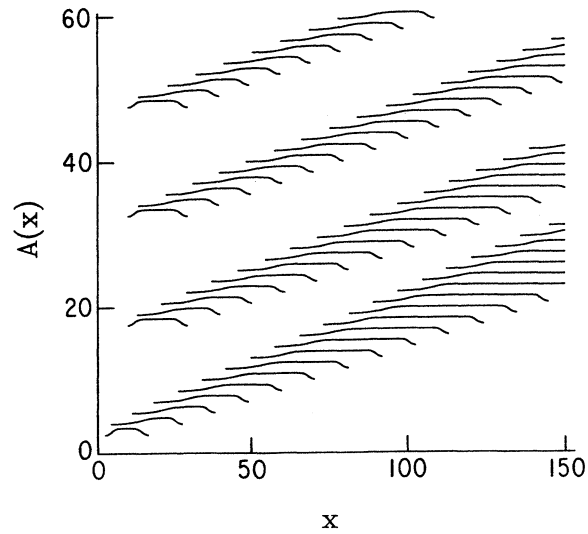

FIG. 8. Propagation of broken-parity bubbles introduced periodically, illustrating a dynamical Maxwell construction. Time increases upward, and successive graphs are displaced upward for clarity. The pattern left in the wake of a given bubble is closer to the coexistence point, as evidenced in the reduced spreading rate of the succeeding bubbles. For clarity, only values of the broken-parity amplitude $A \geq 0.05$ are shown.

4. *Wavelength selection*

The considerations of Sec. III B 3 imply that nucleated inclusions of the broken-parity state generally spread or shrink as they propagate. Here, we investigate the implications of this phenomenon on the dynamics of the phase function ϕ. In order to simplify the analysis, we first motivate a convenient approximation to the amplitude function of a moving inclusion of broken parity. Consider the typical situation (as seen in experiment) of a spreading bubble. When the edges are far apart, the interaction between them is small, and they move with constant velocities. In addition, the widths of the transition zones at the two edges remain constant. Hence, on scales of the order of the length of the bubble, the shape of the envelope function A is reasonably well approximated by a square wave with left and right edges at positions $x_l = v_l t$ and $x_r = v_r t$, v_l and v_r being the propagation velocities of the two edges. They may be computed from the kink-dynamics analysis in previous sections, or simply taken to arise from the particular nonlinearities of a given physical system. Within this approximation, we have

$$A(x,t) \simeq A^* \Theta(x - v_l t)\Theta(v_r t - x) , \tag{3.35}$$

with Θ the Heaviside step function; $\Theta(x) = O(1)$, $x <$ (> 0). In the square-wave approximation, we may solve analytically the phase equation and reveal the nature of wavelength selection.

It is first convenient to recast the phase equation (3.6) in terms of the *phase derivative* $\psi \equiv \varphi_x$ as

$$(\partial_t - D\partial_{xx})\psi = \omega A_x , \tag{3.36}$$

where we have introduced a diffusion constant D for the purposes of later discussion. As in the discussion of kink dynamics in Sec. III B 3, we solve this by means of the diffusion Green's function. The general solution of (3.36) is the sum of the general solution of the homogeneous equation and a particular solution of the inhomogeneous equation. In the simplest case, prior to the creation of the bubble in the amplitude A the phase derivative vanishes identically; the pattern is simply the unperturbed symmetric state. The solution to (3.36) is then immediately analogous to that of Eq. (3.34) in terms of the Green's function

$$G(x,t;x',t') = \Theta(t - t') \frac{1}{2[\pi D(t - t')]^{1/2}} \times \exp\left[-\frac{(x - x')^2}{4D(t - t')} \right], \tag{3.37}$$

satisfying $(\partial_t - D\partial_{xx})G(x,t;x',t') = \delta(x-x')\delta(t-t')$.

Using (3.35), we have

$$A_{x'} \simeq A^*[\delta(x'-v_l t') - \delta(x'-v_r t')] , \tag{3.38}$$

so that the x' integral in (3.34) may be performed trivially. We rescale the x coordinate by the position of the right edge of the bubble and define the parameters

$$\zeta \equiv x/x_r, \quad c \equiv v_l/v_r \quad (0 \le c \le 1) , \tag{3.39}$$

and finally introduce the scaled time

$$\tau \equiv \left[\frac{v_r^2}{4D}\right] t = \frac{x_r v_r}{4D} \tag{3.40}$$

to obtain

$$\psi(x,t) = \frac{\omega A^*}{\pi^{1/2} v_r c}\left[e^{-2\tau c(\zeta-c)} \int_0^{c^2\tau} \frac{dz}{z^{1/2}} \exp\left[-z - \frac{[2\tau c(\zeta-c)]^2}{4z}\right] - c e^{-2\tau(\zeta-1)} \int_0^{\tau} \frac{dz}{z^{1/2}} \exp\left[-z - \frac{[2\tau(\zeta-1)]^2}{4z}\right]\right] . \tag{3.41}$$

For any given rescaled time τ and ratio of velocities c, (3.41) yields the phase derivatives for all ζ (i.e., for all x). Near the onset of the bubble propagation, when the inclusion has not traveled very far compared to the diffusion length D/v_r, the shape of ψ is complicated, reflecting the nonlocality of the Green's function on a scale D/v_r. That nonlocality is reduced by letting $t \to \infty$ ($\tau \to \infty$) in Eq. (3.41), thereby obtaining a *fixed-point* solution for rescaled inclusions that have propagated many phase diffusion lengths. With the identities

$$\int_0^\infty x^{\nu-1} \exp\left[-x - \frac{\mu^2}{4x}\right] dx = 2\left[\frac{\mu}{2}\right]^\nu K_\nu(\mu) \tag{3.42}$$

and

$$K_{1/2}(z) = \left[\frac{\pi}{2z}\right]^{1/2} e^{-z} , \tag{3.43}$$

we obtain

$$\psi \simeq \frac{\omega A^*}{v_r c} \times \begin{cases} 1-c, & 0<\zeta<c \\ -c, & c<\zeta<1 \\ 0, & 1<\zeta. \end{cases} \tag{3.44}$$

Thus, associated with the piecewise constant form of A assumed from the start, there is a piecewise constant phase gradient. Observe that the total phase derivative is conserved,

$$\int_{-\infty}^{\infty} d\zeta\, \psi(\zeta,t) = (1-c)c - c(1-c) = 0 , \tag{3.45}$$

as may be deduced from the equations of motion when $A \neq 0$ only in a finite region. Thus, in this model, cells are neither created nor destroyed. The phase itself may be recovered simply by integration,

$$\phi \simeq \frac{\omega A^*}{v_l v_r} \times \begin{cases} (v_r - v_l)x, & 0<x<v_l t \\ v_l v_r t - v_l x, & v_l t < x < v_r t \\ 0, & v_r t < x. \end{cases} \tag{3.46}$$

An identical result may be obtained simply by ignoring the diffusion term ∂_{xx} in the phase equation and simply integrating in time.

With these results, we conclude that when a bubble of broken parity propagates and spreads in time, and it has moved many diffusion lengths past the point of observation, *the change in the wave vector left behind is proportional to the spreading rate* $v_r - v_l$, which in turn is proportional to the deviation $\mu - \mu^*$. Indeed, the perturbative calculation of Sec. III B 3 yields an explicit value for the wave-vector shift,

$$\phi_x = \frac{75}{2\sqrt{\alpha}} \frac{\omega \Delta\mu}{\gamma^2} , \tag{3.47}$$

ignoring corrections of order ϵ in the average velocity of the kinks.

5. *Wavelength relaxation*

If the passage of a single bubble of broken parity results in a symmetric pattern with an altered wavelength, what effect does the successive passage of additional bubbles have? To answer this, it is necessary first to establish the relative signs of the various parameters of the amplitude equations. It follows from Eq. (3.34) that the structure of the AA_x term is identical to that of the $A\phi_x$ term, and we consider first the simplified model

$$A_t = A_{xx} - \frac{\partial \mathcal{F}}{\partial A} + \epsilon A \phi_x . \tag{3.48}$$

Assume that a bubble moving to the right corresponds to $A > 0$. A derivation similar to that leading to (3.31) then implies that $\epsilon\omega > 0$. This can be deduced by observing that the prefactor $-\gamma$ of (3.31) is replaced by $\epsilon\omega$ as can be seen from (3.34). (Had we chosen the opposite convention for A, then we would conclude that $\epsilon\omega < 0$. However, the freedom of choice for the sign of U_A allows us to reconstruct the identical pattern for the propagating front.)

Using the experimental observation of longer cells within a steadily growing region of asymmetry, the sign of ω may be determined. On either side of the bubble and far from it, the solidification front does not change. In the absence of events that create new cells, phase conservation requires that the wavelength of the pattern left behind will be shorter; that is, behind the bubble $\phi_x > 0$. From Eq. (3.47) it follows that $\omega > 0$. (Had the cells of the asymmetric region been shorter, the same argument

would yield $\omega<0$.) Thus, with the above conventions, we conclude that $\epsilon<0$.

These considerations may be used to explain the wavelength selection law, observation (g) of Sec. II A 1—namely, that successive passage of solitary modes relaxes the pattern to a selected wavelength. Consider the passage of a growing bubble moving to the right. Since the bubble grows, the state $A\neq 0$ is the more stable, and so $\mu>\mu^*$. Further, $\phi_x>0$ for the pattern left behind. Writing (3.48) as

$$A_t=A_{xx}+(\mu^*+\Delta\mu+\epsilon\phi_x)A+\alpha A^3-A^5\cdots , \quad (3.49)$$

we notice that the effective value of μ has changed to

$$\mu'\equiv\mu+\epsilon\phi_x<\mu . \quad (3.50)$$

With $\epsilon<0$ and $\phi_x>0$, the passage of a bubble of broken parity has adjusted the wavelength so that the system is closer to the coexistence point.

From the change in the effective control parameter μ given in (3.50) and the linearity of the equation of motion for the phase, we conclude that successive passages of bubbles of the broken-parity state relax the wavelength to a unique value, according to the map

$$\mu^{(n+1)}=\mu^{(n)}-c|\epsilon|(\mu^{(n)}-\mu^*) , \quad (3.51)$$

where the superscripts denote the value after the nth bubble has passed and c is a numerical constant related to the parameters of the amplitude equations other than ϵ. We may therefore interpret the relaxation phenomenon illustrated in Fig. 8 as an approach to the Maxwell point. *Wavelength selection* occurs by a *dynamical Maxwell construction.*

We should remark that the inclusion of a lateral velocity from terms such as γAA_x in (3.48) may complicate the conclusions drawn above. For instance, if this term is dominant over the velocity arising from the contribution $\epsilon A\phi_x$, then it is not possible to deduce the sign of $\epsilon\omega$ solely on the basis of the sign of the parity bubble velocity. On the other hand, the sign of ω itself is determinable directly from the sign of the phase velocity of the traveling-wave state.

6. *Localized states and dynamical Maxwell constructions*

Once the wavelength of the pattern has relaxed sufficiently, the spreading rate of the bubble is vanishingly small—in a reference frame moving with the center-of-mass velocity of the inclusion, it appears as a *localized state.* In the absence of a coupling between the phase and amplitude, we know from basic considerations that the only configuration of a pair of kinks in A that is stationary is that forming the critical nucleus, and this is an unstable state—larger inclusions grow, smaller ones shrink. In the presence of couplings between the phase and amplitude, the progressive stability of a bubble of fixed length as the phase gradient is altered bears an interesting resemblance to the appearance of localized states in a certain class of reaction-diffusion equations. Here we illustrate the correspondence and a heuristic way of understanding the dynamical Maxwell construction.[25,26]

A well-studied form of reaction-diffusion equation[25] involves an autocatalytic species A and an inhibitor B, the dynamics of the two being given by the rate equations

$$A_t=D_A A_{xx}+f(A)+\epsilon B , \quad (3.52a)$$

$$B_t=D_B B_{xx}+\alpha A-\beta B . \quad (3.52b)$$

The diffusion constants D_A and D_B of the two species in general differ, and the mechanism of localization is most clear when $D_B\gg D_A$, so the species B relaxes on a much faster time scale than does A. The nonlinear term $f(A)$ represents the supposed autocatalytic property of A, and rather generally gives a positive growth of A only for A within some small range centered at a finite value A^*. This nonlinear term may conveniently be written as $f(A)=-\partial F/\partial A$, where

$$F(A)=\tfrac{1}{2}\mu A^2+\tfrac{1}{3}\nu A^3+\tfrac{1}{4}\delta A^4$$

is the usual double-well free energy with two competing minima at $A=0$ and $A\neq 0$. The presence of B in (3.52a) implies inhibitory action if $\epsilon<0$, while (3.52b) reveals that B is stimulated by A but self-limiting (for $\alpha,\beta>0$, as we shall suppose).

In the absence of couplings to the inhibitor field B, the behavior of a localized domain of nonzero A follows classical nucleation theory. When the state $A\neq 0$ is more stable, bubbles smaller than the critical nucleus shrink, while those that are larger grow; no stable finite regions of nonzero A exist. In the presence of B, however, one finds localized states. A heuristic understanding of the stability of these states follows from viewing the quantity $f(A)+\epsilon B$ in (3.52a) as the variation of an effective free energy $F(A)-\epsilon AB$ and thus an effective control parameter $\mu-\epsilon B$. Localized states arise from variations in B that make the nonzero value of A most stable inside the bubble, tending to make its edges move outward, while stabilizing the state $A=0$ outside the bubble. At the center of the kinks the two states are in coexistence and the kink is stationary.

With this analogy, we see clearly that the forms of Eqs. (3.52) and those of the parity-breaking dynamics, (3.4) and (3.6), are very similar, with the phase gradient playing the role of the inhibitor field B. To illustrate the concept of an effective free energy that alters the local stability of the symmetric and broken-parity states, consider the effective control parameter $\mu'=\mu+\epsilon\phi_x$ discussed after Eq. (3.50). Figure 9 shows the deviation $\mu_{\rm eff}\equiv\mu'-\mu^*$ from the Maxwell point as a function of x for a bubble propagating close to wavelength relaxation, clearly showing that the coexistence points ($\mu_{\rm eff}=0$) occur at the bubble edges.

C. Supercritical parity-breaking bifurcations

Here we make several remarks concerning the properties of bifurcations at which the amplitude of broken parity grows continuously from zero at onset. The first and perhaps most important feature of such transitions is that the symmetric pattern becomes *linearly unstable* to broken parity beyond the transition point [$\mu=0$ in Eq. (3.3)]. The entire interface would be expected to become asym-

metric at once, rather than by the nucleation of small regions as in the subcritical case, although under certain circumstances the uniform traveling-wave state may itself be unstable.[20]

Inside any domain with a uniform value of $A \neq 0$, the pattern will be an asymmetric traveling wave with a phase velocity proportional to A. Now, in the supercritical case, the equilibrium values $\pm A^*$ themselves vary as $\sqrt{\mu}$, so we conclude that the phase velocity should scale with the square root of the distance from onset of supercritical parity-breaking bifurcations.

The linear instability of the symmetric pattern beyond onset leads one to expect that the noise in an extended system will generally produce a pattern that is a sequence of domains with an alternating sense of broken parity. The junctions between these regions are elementary defect structures. They necessarily are sources or sinks of traveling waves and new cellular structures and, as such, are the loci of phase singularities and cannot be described by the phase dynamics studied thus far. They are considered in Sec. IV.

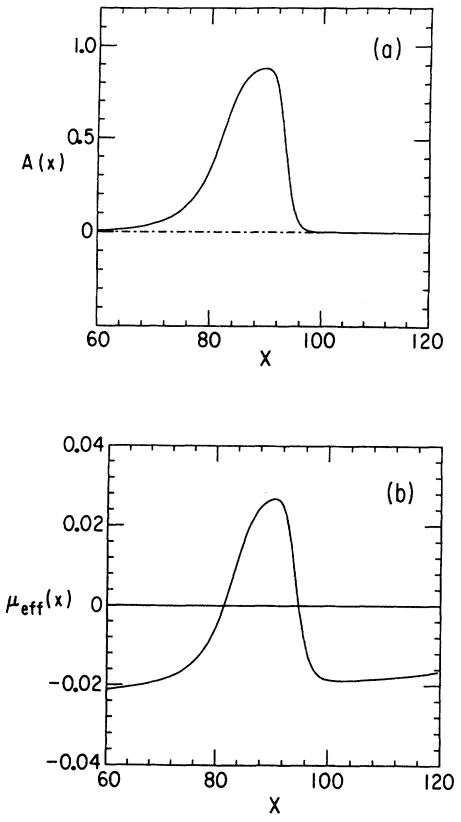

FIG. 9. (a) A bubble of broken parity in a system whose wavelength has relaxed close to coexistence. (b) Effective control parameter $\mu_{\text{eff}} \equiv \mu + \epsilon\phi_x - \mu^*$ as a function of position near the bubble, illustrating that inside the bubble the broken-parity state is favored ($\mu_{\text{eff}} > 0$), while outside the symmetric state is the more stable ($\mu_{\text{eff}} < 0$). Coexistence occurs close to the center of the edges of the bubble in (a).

IV. DEFECT STRUCTURES AND TRAVELING-WAVE STATES

A. Anatomy of a defect

A natural generalization of states with uniformly broken parity is that in which the two dynamically stable traveling-wave states coexist. As shown in Fig. 10, an *interface* between two regions of broken parity (which we refer to as a "defect") is associated with a zero crossing of the order parameter A. The symmetry arguments described in Sec. III allow us to conclude within the present model that, if such a structure exists and the forces on the kinks are such as to push them toward each other, then those forces are equal in magnitude; the defect does not move. How does the phase evolve? Observe that the same nonvariational term in (3.6) that leads to a phase evolution $\phi = \pm\omega A^* t$ far from the defect—that is, traveling waves with opposite propagation directions corresponding to the opposite sign of the broken parity—of necessity leads to an arbitrarily large *phase gradient* at the core of the defect. This continual growth of the phase gradient would imply that within any neighborhood of the defect there would be an ever-increasing number of cellular structures of ever-decreasing wavelength.

Such a continual spatial contraction quite generally leads to a destabilization of the pattern, typically by means of the Eckhaus instability,[27] a dynamical process not contained in the phase evolution discussed in Sec. III. Note further that the absolute value of the phase of the pattern is irrelevant, only its value modulo 2π is relevant, a consideration most naturally contained in a description in which the phase is associated with the argument of a *complex order parameter.* We propose[9] in this section that a description of the dynamics of defects of broken-parity states may be formulated by a suitable coupling between the *scalar* amplitide A of the broken parity and a *complex* order parameter B associated with the sym-

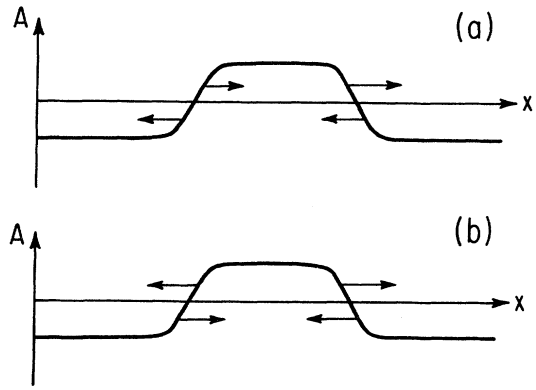

FIG. 10. Interfaces between regions of broken parity as described by the order parameter A. Arrows indicate the direction of forcing on the kinks. Two regimes may be distinguished: (a) advection-dominated—only one type of defect (the right-hand one) is stable; (b) spreading-dominated—both sources and sinks of traveling waves are stable.

metric component of the pattern, with $\arg(B)=\phi$. In order to elucidate the effects of differential forcing at a defect, it is useful first (Sec. IV B) to eliminate the dynamics of the kink-shaped forcing function $A(x)$ (Fig. 10) and replace it with a static function, leading to a spatially forced Ginzburg-Landau model of a periodic pattern. With the insight thus gained, a phenomenological model with couplings between A ands B is proposed that allows for a consistent description of the dynamics of defects in three important contexts. First, we consider an isolated defect at the junction between two semi-infinite regions of broken parity and demonstrate that viewed as a function of space and time, such a junction is a "spatiotemporal grain boundary," the core of which is a locus of "spatiotemporal dislocations" which correspond to the creation or destruction of new cellular structures. Second, there may exist patterns consisting of alternating sources and sinks. Finally, the dynamics of collisions between two finite regions of opposite broken parity, and in particular the empirical rule of length subtraction described in Sec. II, follow directly from these results.

B. A spatially forced complex amplitude equation

Consider a system with a supercritical primary instability leading to a stationary periodic pattern and let ν be a dimensionless control parameter defined as positive beyond the instability. Near onset, the dynamics of the pattern U may be reduced to that of a complex amplitude $B(x,t)$, where by a suitable rescaling of space,

$$U \simeq \tfrac{1}{2}(Be^{ix}+B^{*}e^{+ix})+\cdots , \tag{4.1}$$

with B^{*} the complex conjugate of B, the ellipses representing higher harmonics. A canonical form for the dynamics of B is $B_t=B_{xx}+\nu B-|B|^2B$. In the presence of a *real* forcing $g(x)$ that acts solely on the phase of B, we obtain

$$B_t=B_{xx}+\nu B-|B|^2B+ig(x)B . \tag{4.2}$$

A particularly simple form for g is

$$g(x)=g_0\tanh(x/\delta) , \tag{4.3}$$

the defect being located at the origin.

Provided $|B|\neq 0$, it is meaningful to write $B=S\exp(i\phi)$ and so to deduce the coupled dynamics

$$\begin{aligned} S_t &= S_{xx}+(\nu-\phi_x^2)S-S^3 , \\ \phi_t &= \phi_{xx}+2S^{-1}S_x\phi_x+g . \end{aligned} \tag{4.4}$$

This phase equation is then the generalization of (3.6) to a complex order parameter with spatially varying magnitude. As the amplitude dynamics in (4.4) reveal; here, unlike in models that do not respect the periodicity of the phase, the large phase gradients produced by $g(x)$ at the origin destabilize the pattern. This destabilization is reminiscent of the Eckhaus instability exhibited by B in the presence of *homogeneous* forcing, whereby the state with wave-vector mismatch Q (i.e., $\phi=Qx$) and with amplitude $S=(\nu-Q^2)^{1/2}$ becomes unstable for $Q^2>\nu/3$ and ceases to exist for $Q^2>\nu$.

How does the system evolve from the initial equilibrium state in which the pattern is uniformly in the center of the band of stable states, i.e., $S=\nu^{1/2}$, $\phi=0$? Figures 11 and 12 show the results of numerical integration[24] of (4.2), in which we write $B=u+iv$ and solve the equations

$$\begin{aligned} u_t &= u_{xx}+\nu u-(u^2+v^2)u-gv , \\ v_t &= v_{xx}+\nu v=(u^2+v^2)v+gu \end{aligned} \tag{4.5}$$

for $u(x,t)$ and $v(x,t)$, rather than employ the polar decomposition. Far on either side of the defect, the forcing is homogeneous and we obtain the simple results

$$u(x,t)=\sqrt{\nu}\cos(g_0t),\quad v(x,t)=\sqrt{\nu}\sin(g_0t) \qquad (x\to+\infty) , \tag{4.6a}$$

$$u(x,t)=\sqrt{\nu}\cos(g_0t),\quad v(x,t)=-\sqrt{\nu}\sin(g_0t) \qquad (x\to-\infty) . \tag{4.6b}$$

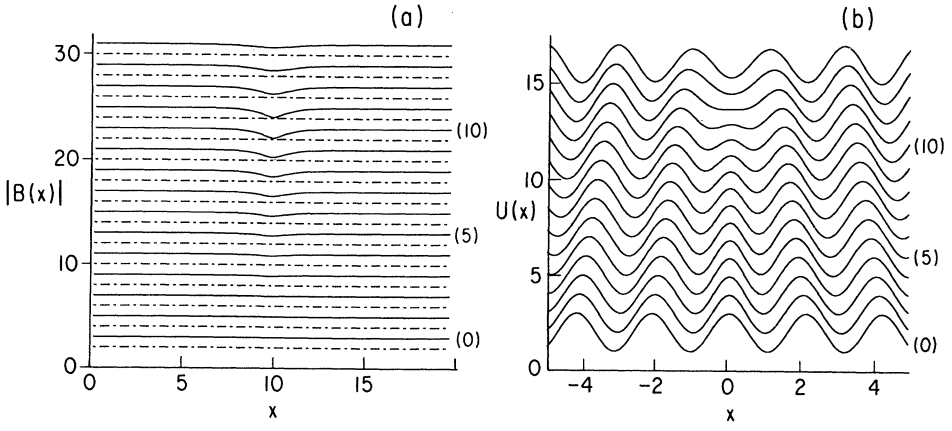

FIG. 11. Evolution of a spatially forced Ginzburg-Landau model, with time increasing upward. (a) $|B(0,t)|$ vanishes periodically. (b) The reconstructed pattern shows that this vanishing corresponds to the disappearance of a cell. Numbers beside the successive graphs correspond to those in Fig. 12.

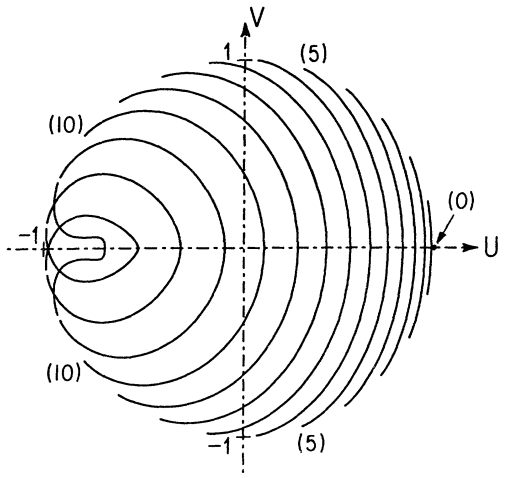

FIG. 12. Phase portrait of the forced Ginzburg-Landau equation at successive points in time, with spatial coordinate x parametrizing the curves. The destruction of a cell corresponds to the simultaneous vanishing of the real and imaginary parts of $B=u+iv$. Numbers beside curves correspond to Fig. 11.

Near the defect, the evolution is consistently more complex. As the initially uniform state develops a phase gradient near $x=0$, the modulus of B steadily decreases until both the real and imaginary parts smoothly cross through zero, as shown in Fig. 11(a). An alternate way to view this is by means of a phase portrait in the u-v plane, with the spatial variable x parametrizing the curve, shown in Fig. 12.

The vanishing of B at the defect is found to be *periodic in time,* the frequency related to the rate ω at which the phase gradient grows to destabilize the pattern. The reconstructed pattern

$$U(x,t)=u(x,t)\cos(x)-v(x,t)\sin(x) , \tag{4.7}$$

shown in Fig. 11(b), reveals that this periodic zero of B corresponds to the destruction of a cell, consistent with the defect being a sink of traveling waves. Had we chosen g_0 of the opposite sign, the defect would be a source of traveling waves, a locus of new cells.

C. Dynamics with couplings between symmetric and antisymmetric components

1. A generalized model

Having established that a differentially forced complex order parameter avoids large phase gradients by vanishing periodically, we return to patterns with broken parity and develop a model for the dynamics of a defect. We consider again the model equations for the amplitude of broken parity and the phase of the pattern,

$$A_t=A_{xx}-\frac{\partial F}{\partial A}+\gamma A A_x+\epsilon A\phi_x+\cdots , \tag{4.8a}$$

$$\phi_t=\phi_{xx}+\omega A+\cdots , \tag{4.8b}$$

and generalize them to the case in which ϕ is the argument of a complex field B, and in which the primary instability that breaks the continuous translational invariance is supercritical, as in Sec. IV B.

With the proposed representation of the amplitude of the symmetric component of the pattern with a complex field B and that of the antisymmetric component with a scalar field A, we demand of the dynamics invariance under the transformations

$$x\to -x, \quad A\to -A, \quad B\to B^* . \tag{4.9}$$

From the discussion around Eq. (4.2), it is clear that the appropriate dynamics for B is

$$B_t=B_{xx}+\nu B+|B|^2B+i\omega AB . \tag{4.10}$$

To generalize the term $A\phi_x$ in (4.8a), observe that the phase gradient is

$$2S^2\phi_x=i(B^*B_x-BB_x^*) , \tag{4.11}$$

very much like the *probability current* in quantum mechanics (with B representing the wave function). Indeed, as we discuss in Sec. IV D below, there is a strong analogy to be made with the dynamics of superfluids and superconductors.

Viewing ν as the basic control parameter (e.g., in directional solidification, $\nu\propto v-v_{\rm MS}$, where v is the imposed forward velocity of the interface and $v_{\rm MS}$ is that of the Mullins-Sekerka instability), we make the plausible assumption that the control parameter μ in the dynamics of A varies primarily through the growth in the amplitude of the symmetric component, and hence implicitly with ν. To lowest order, this implies that the effective μ increases linearly in $|B|^2$. We thus arrive at the model

$$A_t=A_{xx}+(\tilde{\mu}+|B|^2)A+\alpha A^3-A^5 +i\frac{\epsilon}{2}(BB_x^*-B^*B_x)A+\gamma A A_x . \tag{4.12}$$

In a polar decomposition, with $B=Re^{i\varphi}$, (4.10) and (4.12) become

$$\begin{aligned} R_t&=R_{xx}+(\nu-\varphi_x^2)R-R^3 ,\\ \varphi_t&=\varphi_{xx}+2\frac{R_x}{R}\varphi_x+\omega A , \\ A_t&=A_{xx}+(\mu+R^2)A+\alpha A^3-A^5+\epsilon R^2\phi_x A . \end{aligned} \tag{4.13}$$

The remaining parameters δ, μ, α, etc., are taken to be fixed. For $\mu+|B|^2>\mu^*$ the broken-parity state becomes dynamically stable, and from a linear stability analysis around the state $A=0$, $\phi=Qx$, $B=(\nu-Q^2)^{1/2}$, we may locate the stability boundary for broken parity shown in Fig. 4 in the space of ν and phase gradient Q. A schematic neutral stability diagram is shown in Fig. 13 for the case $\epsilon>0$. Observe that the parity-breaking bifurcation curve intersects the vertical axis at an angle. This implies that a quench of the system to a state with a uniform phase gradient Q will lead to nucleation of parity-breaking modes only if the *sign* of the jump in Q is ap-

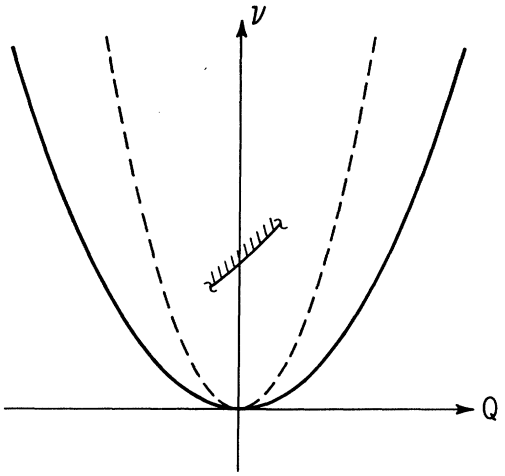

FIG. 13. Schematic stability diagram including the Eckhaus (dashed) and parity-breaking instabilities (hatched region).

propriate (negative in the case shown in the figure). This behavior is in accord with experiments on directional solidification.[2,3]

2. *Analogy with superconductors in applied electric fields*

As remarked above, the dynamics of the complex symmetric order parameter in Eq. (4.10) bears a strong relation to that found in superconductors, an analogy that is made more complete here. Recall the essential aspects of the time-dependent Ginzburg-Landau (TDGL) description of the dynamics of a superconductor.[28] The TDGL equation in the absence of a vector potential is

$$\left[\frac{\partial}{\partial t}+\frac{2i\mu_e}{\hbar}\right]\psi=\frac{\partial^2}{\partial x^2}\psi+r\psi-|\psi|^2\psi\ , \tag{4.14}$$

where $\psi(x,t)$ is the complex superconducting order parameter. μ_e is the electrochemical potential related to the electrostatic potential V by[29]

$$\mu_e \simeq eV\ , \tag{4.15}$$

with a suitable definition of the reference of chemical potential.

With $\psi=\chi\exp(i\phi)$ we have, as in (4.10),

$$\chi_t=\chi_{xx}+(\nu-\phi_x^2)\chi-\chi^3\ , \tag{4.16a}$$

$$\phi_t=\phi_{xx}+\chi^{-1}\chi_x\phi_x-\frac{2\mu_e}{\hbar}\ , \tag{4.16b}$$

the latter being the Josephson relation.[30] In this form, we see that the traveling-wave relation $\phi_t\simeq\omega A$ is essentially also a Josephson relation, with the broken-parity order parameter corresponding to the electrochemical potential. In the parity-breaking problem, of course, there are no universal scale factors analogous to $\hbar$ that enter the Ginzburg-Landau (amplitude) equation, but nevertheless there are certain universal features that can be tested experimentally. Most importantly, as remarked earlier, *for supercritical bifurcations* the growth of the amplitude of broken parity near onset, $A\sim\nu^{1/2}$, implies the generalized Josephson relation connecting the phase velocity v_p and the control parameter

$$v_p\simeq v_0\nu^{1/2}\ , \tag{4.17}$$

v_0 being some nonuniversal constant

3. *Propagating inclusions*

With the coupled dynamics of (4.12), we return to the motion of propagating inclusions of the broken-parity state and recall that the symmetric pattern left in the wake of such a bubble has a wavelength shortened from that before the bubble passed, provided the bubble is spreading. In the context of the couplings proposed above, where the phase gradient and the symmetric amplitude are coupled, it follows that *the amplitude of the symmetric pattern remaining is diminished as well.* Note also that with the essentially triangular shape of the phase function that arises from the propagation of a parity bubble, there may be an instability of the pattern *within the inclusion* if the phase gradient there is too large. That is, the propagation of a parity bubble may lead to a spontaneous creation of new cells. Near the top left of Fig. 1(a) we see such an event in the case of solidification.[31] There is additional evidence for this phenomenon in directional viscous fingering.[32]

4. *Spatiotemporal grain boundaries, spatiotemporal dislocations, sources, and sinks*

There are two fundamental kinds of boundaries between adjacent regions of opposite broken parity, distinguished by their handedness, as in Fig. 10. The sign of the coupling constant ω in the phase relation $\phi_t=\phi_{xx}+\omega A$ determines whether a given defect acts as a source or sink of traveling waves. It was established in Sec. III that the symmetries of the equations of motion require that kinks with opposite parity and orientation move with velocities of equal magnitude but opposite sign. Thus, in isolation, both junctions are forced equally from both sides, and therefore do not move. On the other hand, the stabilities of the two defects are not identical. As remarked in the discussion of kink dynamics in Sec. III B, the dynamical forcings on kinks can lead to two qualitatively different regimes for the motion of bubbles of broken parity: (i) advection dominated and (ii) spreading dominated. In the former, as shown in Fig. 10, only one kind of defect is stable. In the latter case, both are stable.

Far beyond the hysteretic region of a subcritical bifurcation, or beyond the onset of a supercritical bifurcation, we expect the rate of expansion of bubbles of broken parity to overwhelm other forcing, and the system to be in regime (ii). Figure 14 shows reconstructions of the two kinds of spatiotemporal grain boundaries, sources, and sinks, for a system far beyond onset. We see that far from the defect the pattern is a uniform traveling wave, but there are distortions in the phase velocity close to the defect as the broken-parity order parameter approaches zero.

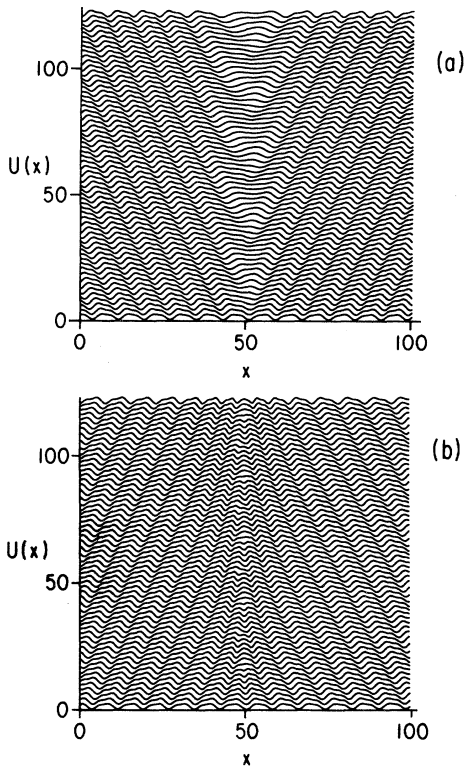

FIG. 14. Two types of spatiotemporal grain boundaries in the spreading-dominated regime. (a) A source of traveling waves; (b) a sink.

In situations where both sources and sinks are stable, we may anticipate that a pattern prepared with arbitrary initial conditions may develop an alternating sequence of sources and sinks, separated by somewhat random intervals. Experiments on directional viscous fingering indicate that this is the case.[32] Such a pattern is reminiscent of the "phase slip oscillator," state[33] discussed in the context of superconductivity, in which there is a spatial array of sites at which the superconducting order parameter is periodically driven to zero. We defer a detailed discussion of the interactions between these defects, but remark here that experiments[31] indicate the possibility of a bound state of two defects.

5. *Collisions*

The dynamics of phase slips at the junctions between regions of opposite broken parity allows us to understand the nature of collisions between parity bubbles, and in particular the creation of new cells and the origin of the empirical rule of length subtraction. Figures 15 and 16 illustrate the dynamics of annihilating and partially annihilating collisions as deduced from the model (4.10) and (4.12). The junction between two finite domains of oppositely broken parity is essentially a transient grain boundary, the order parameter A locally having the shape of the kink connecting the two states $\pm A^*$. This junction remains fixed in space during the course of the collision, as a consequence of the equal and opposite variational and nonvariational forcing on its two halves, but the two outer edges of the bubbles continue traveling inward with velocities of equal magnitude. The transient occurrence of a kinklike structure connecting the states $\pm A^*$ leads to a periodic phase instability (or several) at the junction, and this yields new cellular structures. When viewed in terms of, say, the maxima of the pattern U in Figs. 15(b) and 16(b), these instabilities during a collision are "spatiotemporal dislocations." Once the outer edge of the shorter bubble gets close to the junction, that bubble will become smaller than the critical nucleus and thus collapses to zero, leaving the remainder of the longer domain to propagate in its original direction, slowly spreading as before. It follows that the rule of length subtraction is approximate up to deviations on the order of the critical nucleus.

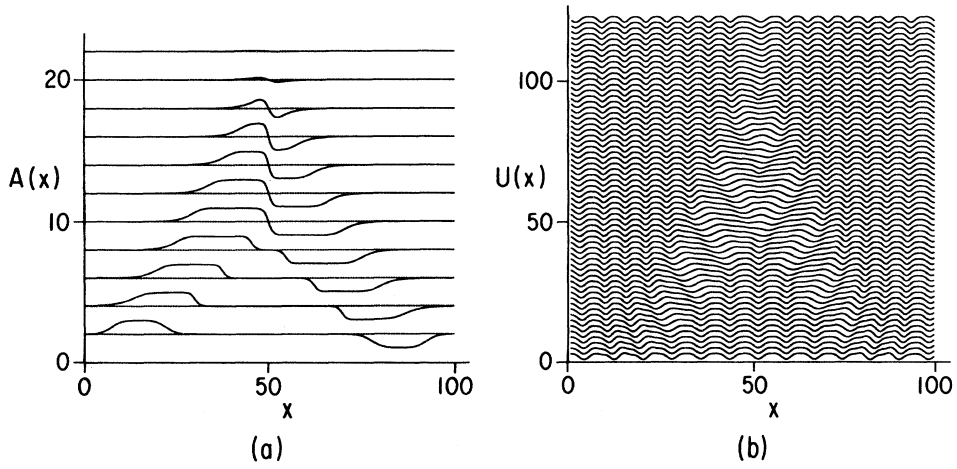

FIG. 15. Annihilating collision between broken-parity domains of equal length. The reconstructed interface pattern U in (b) is calculated from the broken-parity order parameter in (a). For clarity, the latter is shown at one-tenth the temporal resolution used in (b).

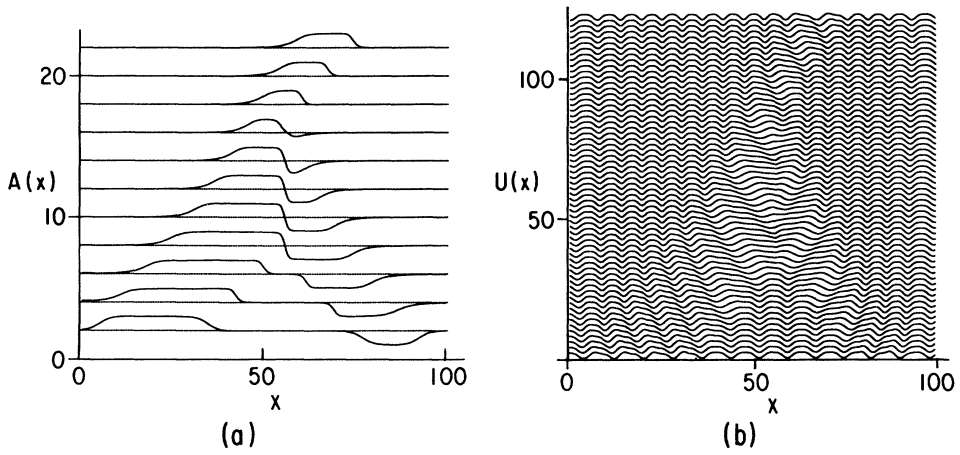

FIG. 16. Same as in Fig. 15, but a partially annihilating collision.

V. SUMMARY OF COMPARISONS WITH EXPERIMENTS

Modulated hydrodynamic states destabilize by breaking one or more of their symmetries. We have suggested the breaking of parity symmetry as a possible explanation of the experimental observations summarized in Sec. II. The universality of the features, in spite of the diverse nature of the physics, suggests that they are indeed properties of a common transition. Their strong resemblance to properties of the model advanced here suggests that the experimental systems exhibit such bifurcations. The following brief summary of comparisons with experiments is oriented toward the directional solidification experiments on liquid crystals (see Sec. II A 1), for which the most detailed information is available.

The experimental observation of a first-order transition was built into the theory, and in Sec. III B 5 several simple observations were used to determine the signs and ranges of the model parameters μ, ϵ and ω. The remaining observations of Sec. II follow from the model: The velocity $v_2(G)$ at which solitary modes first propagate freely corresponds to the Maxwell point, beyond which the asymmetric state is the more stable. The form of the nonvariational terms in Eqs. (3.4) and (3.6) implies a precise correlation between the sign of the asymmetry and the direction of motion of the solitary mode. Further, it follows from Eqs. (3.31) and (3.33) that the velocity of a solitary mode is independent of its length (provided that it is sufficiently longer than the critical nucleus) and is a function only of μ and ϵ, and hence varies only with the forward velocity of the interface and the applied temperature gradient. The wavelength relaxation rule (g) follows directly from the model, as discussed in Sec. II A 5.

In both directional solidification and Rayleigh-Bénard experiments the fundamental selected wavelengths of the symmetric cellular pattern is a decreasing function of the control parameter (forward interface velocity or applied temperature difference). Associated with this shrinking of the pattern is the observation that velocity quenches of size Δv nucleate new cellular structures by means of asymmetric traveling domains generally only if $\Delta v > 0$. This onesidedness suggests clearly that the stability of the antisymmetric state depends on the *sign* of the mismatch between the wave vector of the pattern and the one to which it is relaxing after the quench. The symmetry considerations associated with parity-breaking bifurcations in general require that this be the case.

The approximate length subtraction rule (h) and the creation of new cells at the interface (i) are consequences of the model of Sec. III and the interpretation of the collision front as a phase slip center. Close to the coexistence region, only sinks are stable, while farther away, both sources and sinks can exist.

To elucidate further the nature of parity-breaking transitions, we raise the following questions as experimental tests.

(i) Resolve the experimental pattern into symmetric and antisymmetric components and thereby deduce the broken-parity order parameter and slowly varying phase. What are the length scales for the variations of A and ϕ?

(ii) For velocities far beyond the onset of broken parity, do solitary modes expand in both directions and ultimately cover the entire interface?

(iii) Near the supercritical parity-breaking bifurcation, does the phase velocity vary with the broken parity as expected [Eq. (4.17)]?

(iv) At a source of traveling waves, does the symmetric component of the pattern vanish periodically at the same rate as the creation of new cells (the Josephson relation)?

VI. EXTENSIONS

More recent experiments[31] on directional solidification of liquid crystals have been carried out in containers whose lateral extent L is only on the order of ten cells wide, thus affording the opportunity to address the nature of geometric pattern selection in these systems. As is often found in confined hydrodynamic systems, the boundary conditions on the interface resemble closely those found in equilibrium situations, meaning here that there is a reasonably constant contact angle as a function

of the forward velocity v of the interface. Consequently, there is an integral number of cells between the walls; the wave vector $q_0(v)$ of the periodic pattern is *quantized.* Figure 17 illustrates this wavelength locking phenomenon, contrasting sharply with the continuous variation $q_0(v)$ found in containers with $L/\lambda_0 \gg 1$.

The relevance of a parity-breaking instability to this geometric quantization appears in the dynamical mechanism by which a pattern with n cells adds a cell upon a gradual increase of the forward velocity v. Provided $L/\lambda_0 \geq 5$ (i.e., that the central region of the pattern is unaffected by the walls), it is found[31] that such an increase in the wave vector q is achieved by the nucleation of a solitary mode, typically at one or the other wall in the system. This inclusion may travel across the length of the container, increase the wave vector of the pattern left behind, as in unconfined geometries. Remarkably, this parity-breaking phenomenon appears at the edge of *each* of the plateaus in the q-v plane of Fig. 17, in contrast to the situation in an infinite container where it occurs at a unique velocity.

Interestingly, there is a fundamental asymmetry in the mechanism by which wavelength changes occur when one compares *increases* and *decreases* of the control velocity v. That is, the nucleation of solitary modes that occurs with increasing v is replaced by an Eckhaus-like instability that is responsible for destroying cellular structures upon decreasing v. This is reminiscent of the features of the stability diagram derived in Sec. IV, shown schematically in Fig. 13.

The appearance of a parity-breaking instability along each of the plateaus of constant wave vector may be understood[34] by viewing the *mismatch* between the geometrically selected wave vector and the one selected in an infinite system as a negative phase gradient that changes the effective control parameter for the bifurcation from μ to $\mu+\epsilon\phi_x$. If, as established in previous sections, $\epsilon<0$, then such a phase gradient will destabilize the symmetric pattern. Similarly, progressive decrease in the forward interface velocity will lead to a positive phase gradient that would eventually destabilize the interface by an Eckhaus-like mechanism without an intervening parity-breaking bifurcation.

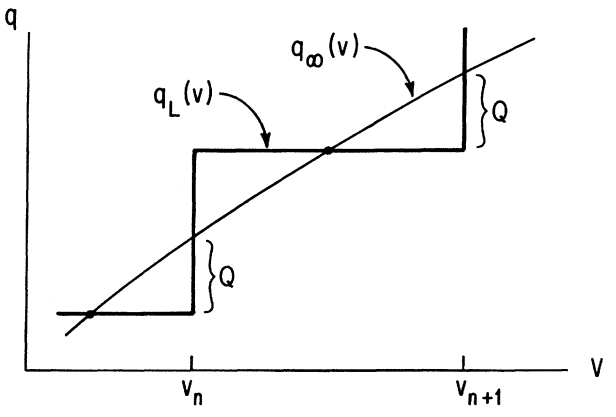

FIG. 17. Diagram illustrating effects of confined geometries. The observed wave vectors in narrow channels are discrete, whereas in the infinite system they form the continuous function $q_0(v)$, with v the imposed forward interface velocity. Velocities v_n are those at which the system undergoes a transition from n to $(n+1)$ cells.

Nowhere in the discussion above have we taken into account the existence of liquid-crystalline order within the nematic phase of the directional solidifcation experiments. On a gross level, one might imagine that the only indication of those degrees of freedom is the particular values of the material parameters such as the capillary length, latent heat of transition, partition coefficient, etc., and also therefore in the coefficients of the Ginzburg-Landau model for parity breaking. On the other hand, recent experiments[14] have indicated that there may be an intimate connection between certain *defect structures* associated with the nematic director and the motion of the nematic-isotropic interface itself.

It is known[35] that the director in these liquid crystals tends to lie at a particular orientation with respect to the nematic-isotropic interface—in some systems it is normal to the meniscus, in others at an angle. In any fully microscopic description of the solidification dynamics, we might expect that the complex nematodynamics would supplement the usual thermal and/or impurity diffusion. Likewise, in a long-wavelength approach based on symmetries and invariances, it is natural to ask whether the existence of nematic order might alter the form of amplitude equations. One possibility, analogous to that in smectic liquid crystals,[36] is that a joint rotation of the director and the nematic-isotropic interface does not alter the properties of the system (in the absence of a symmetry-breaking thermal gradient); only the *relative* gradients of the interface position and nematic director are important. Thus, spatial derivatives in amplitude equations would become *covariant;* the nematic order would induce a "gauge field." As is the case for flux lattices in superconductors, the existence of such an auxiliary field can lead to important defect structures. That such a gauge field might exist has been conjectured recently[37] in the context of electrohydrodynamic convection in liquid crystals, but it is an important open problem to determine whether the director does indeed play the role of a gauge field in these one-dimensional patterns.

VII. DISCUSSION

The qualitative agreement between the dynamics of the simplified model of a parity-breaking transition and the experimental observations, particularly in directional solidification, reveals the power and generality of symmetry arguments. Yet, out of this analysis comes no *microscopic* understanding of the mechanisms that produce these instabilities. Here, we discuss possible origins for the ubiquity of parity-breaking bifurcations in dissipative pattern-forming systems.

In Sec. II B we outlined some of the important common features of the experimental systems, and in particular the indications that the second harmonic of the mode that appears at onset plays an important role. Note that such a harmonic content cannot arise from underlying dynamics of the form

$$U_t = f(U) \tag{7.1}$$

if $f(U)$ is an odd function of its argument, as is the case, for instance, of the Swift-Hohenberg[38] equation

$$U_t = -rU - 2U_{xx} - U_{xxxx} - U^3 \ . \tag{7.2}$$

The cubic nonlinearities in (7.2) will only mix odd harmonics like $\cos(q_0 x)$ and $\cos(3q_0 x)$. Clearly, even-order nonlinearities are needed, the lowest-order such terms being quadratic. It is precisely these even nonlinearities that remove the symmetry between U and $-U$, a symmetry that is known[39] to be broken in the case of directional solidification. In convection at large Rayleigh numbers, the fluid properties at the top and bottom of the convective cell would differ, thus breaking the up-down symmetry of the velocity profile in the convective rolls. Such effects might indicate a breakdown of the Boussinesq approximation.[40]

The first part of our conjecture is then that parity-breaking bifurcations may arise as a consequence of dynamics which break the "up-down" ($U \rightarrow -U$) symmetry and thereby nonlinearly couple the fundamental mode and the second harmonic.[41]

Why should the generation of the second harmonic of a cellular pattern lead to a secondary instability (Ref. 42)? One possible answer comes from considering again the linear stability of the homogeneous pattern. As can be seen in Fig. 2, in which we have drawn interfacial patterns corresponding to the form

$$U_S(x) = b_1 \cos(q_0 x) + b_2 \cos(2q_0 x) \ ,$$

with $b_2/b_1 = -0.25$, growth of the second harmonic creates a pattern that is progressively flatter at its leading edge. By the time the ratio of amplitudes is like that in Fig. 2(a), the front of the interface is nearly flat, and its stability might plausibly be understood in terms of an analysis around the planar state. Sufficiently far beyond the onset of the primary instability, the band of unstable modes may contain the mode of wave vector $2q_0$; the positive growth rate for this second harmonic may then signal a secondary bifurcation of the periodic pattern.

From the results in previous sections, it is clear that a fundamental aspect of the dynamics of broken parity is the lack of a variational principle governing the normal form expansion. This suggests that the underlying microscopic equations of motion also involve nonvariational terms. In both solidification and viscous fingering experiments the underlying equations of motion for the spatially distributed fields are either diffusive or Laplacian, and *linear*. The origin of all of the nonlinearities lies in the boundary conditions on those fields. In both of these cases, the boundary conditions involve relationships between the interface position, curvature, and normal derivatives. Fundamental to these geometric features of the interface is the metric relationship between arc length and the shape of the boundary

$$ds = (1 + U_x^2)^{1/2} dx \ . \tag{7.3}$$

Both the "geometric"[43] and "boundary-layer"[44] models of solidification suggest that the nonlinearities embodied in the metric might enter directly into the equations of motion of interfaces.

That nonvariational quadratic nonlinearities such as U_x^2 might play a role in secondary instabilities of periodic patterns has been discussed[45] in the context of a modified version of the Kuramoto-Sivashinsky (KS) equation,[46] which also finds application in the study of flame fronts and other nonequilibrium systems. A convenient form of the KS equation is

$$U_t = -rU - 2\alpha U_{xx} - U_{xxxx} + \nu U_x^2 \ . \tag{7.4}$$

This equation is also obtainable from the "geometric" model of solidification, and directly from the underlying microscopic physics[47] and boundary conditions. The linear stability of the homogeneous pattern $U = \text{const}$ to perturbations of the form $U = \exp(ikx + \sigma t)$ yields a growth rate curve $\sigma(k)$ that has the essential features for solidification: a quadratic maximum at some finite wave vector k_0, with both damping at the extremes of low and high wave vectors.

As discussed elsewhere,[48] the cellular structures found near the onset of the primary instability of the homogeneous interface remain left-right symmetric over a range of control parameter beyond that onset. There is a well-defined point, however, where the parity is broken. In a simplified treatment,[45] the interface function is approximated by a linear combination of a small number of modes, the amplitudes of which constitute a reduced set of dynamical variables,

$$U(x,t) \simeq B_1 \cos(q_0 x + \phi) + B_2 \cos[2(q_0 x + \phi)] + A_2 \sin[2(q_0 x + \phi)] + \cdots \ . \tag{7.5}$$

As expected, the second harmonic of the basic pattern arises from the quadratic nonlinearity and leads to cellular structures that are quite reminiscent of those seen in experiment. Further analysis suggests that when the band of unstable modes in the stability analysis of the homogeneous state is broad enough, the broken-parity amplitude A_2 becomes finite. This point roughly corresponds to that at which the growth rate of the second harmonic becomes positive. At this instability, the phase becomes a propagating mode, so the pattern exhibits traveling waves. Interestingly, then, the lowest-order quadratic nonvariational nonlinearity consistent with the underlying $x \rightarrow -x$ symmetry of the equations of motion leads to a parity-breaking transition. A normal form analysis of this bifurcation[41] should prove illuminating in the study of parity-breaking bifurcations and may serve as a check of the ideas advanced here.

Finally, given a simple microscopic model for a subcritical bifurcation, it may be possible to address the origin of the *hydrodynamic noise* that ultimately nucleates the new state. In this issue, also, we may expect the existence of nonvariational dynamics to play an important role. As is well known, when the microscopic equation of motion is variational, $U_t = -\delta \mathcal{F}/\delta U$, then $\mathcal{F}$ itself is a nonincreasing function of time, and the system is continually relaxing to a (perhaps metastable) minimum of $\mathcal{F}$. Such unidirectional relaxation does not exist for nonvariational dynamics, and its absence is clearly seen in nu-

merical simulations[49] of the KS equation. Perhaps a study of nucleation at a subcritical bifurcation in the context of nonvariational dynamics will be a fruitful step toward understanding the origin and magnitude of hydrodynamic noise.

ACKNOWLEDGMENTS

We are grateful to our colleagues G. Iooss, Leo P. Kadanoff, Albert Libchaber, and Adam Simon for a fruitful collaboration, and to J. Bechhoefer, Y. Couder, S. de Cheveigne, M. Dubois, S. Fauve, J.-M. Flesselles, V. Hakim, P. C. Hohenberg, A. P. Kast, J. S. Langer, S. Leibler, H. Levine, J. Palmieri, I. Procaccia, H. Riecke, and W. van Saarloos for important insights. This work was supported in part by National Science Foundation (NSF) Grant No. CHE-8808378 (R.E.G.), the Office of Naval Research (G.H.G.), and the Direction de la Recherche et des Etudes Techniques (L.G.). R.E.G. gratefully acknowledges the hospitality of the Université de Nice and the Centre d'Etudes Nucleaires de Saclay during extended visits.

---

*Present address: Department of Physics, Jadwin Hall, Princeton University, Princeton, NJ 08544.

†Present address: Department of Physics, University of Houston, Houston, TX 77204.

[1]W. W. Mullins and R. F. Sekerka, J. Appl. Phys. **34**, 323 (1963); **35**, 444 (1964).

[2]A. J. Simon, J. Bechhoefer, and A. Libchaber, Phys. Rev. Lett. **61**, 2574 (1988).

[3]G. Faivre, S. de Cheveigne, C. Guthmann, and P. Kurowski, Europhys. Lett. **9**, 779 (1989).

[4]M. Rabaud, S. Michalland, and Y. Couder, Phys. Rev. Lett. **64**, 184 (1990); see also I. Mutabazi, J. J. Hegseth, C. D. Andereck, and J. E. Wesfreid, Phys. Rev. Lett. **64**, 1729 (1990).

[5]F. Daviaud, M. Bonetti, and M. Dubois Phys. Rev. A **42**, 4338 (1990).

[6]F. Melo and P. Oswald, Phys. Rev. Lett. **64**, 1381 (1990).

[7]S. Douady, S. Fauve, and O. Thaul, Europhys. Lett. **10**, 309 (1989); see also Ref. 17.

[8]P. Coullet, R. E. Goldstein, and G. H. Gunaratne, Phys. Rev. Lett. **63**, 1954 (1989).

[9]R. E. Goldstein, G. H. Gunaratne, and L. Gil, Phys. Rev. A **41**, 5731 (1990).

[10]P. Coullet and G. Iooss, Phys. Rev. Lett. **64**, 866 (1990).

[11]A. C. Newell and J. A. Whitehead, J. Fluid Mech. **38**, 279 (1969).

[12]In recent work [H. Levine, W.-J. Rappel, and H. Riecke, Phys. Rev. A **43**, 1122 (1991)] , the conjecture of a parity-breaking bifurcation advanced in Ref. 8 has been verified within a numerical study of the fully nonlinear and nonlocal dynamics appropriate to directional solidification. See also P. Haug, Phys. Rev. A **35**, 4364 (1987); **40**, 7253 (1989) for a discussion of mode interactions in directional solidification dynamics.

[13]P. Oswald, J. Bechhoefer, and A. Libchaber, Phys. Rev. Lett. **58**, 2318 (1987).

[14]A. J. Simon and A. Libchaber (unpublished).

[15]See also H. E. Cline, Mater. Sci. Eng. **65**, 93 (1984); Metall. Trans. A **15**, 1013 (1984).

[16]K. .A. Jackson and J. D. Hunt, Trans. AIME **236**, 1129 (1966); see also K. Brattkus, B. Caroli, C. Caroli, and B. Roulet, J. Phys. (Paris) **51**, 1847 (1990); B. Caroli, C. Caroli, and B. Roulet, *ibid.* **51**, 1865 (1990).

[17]It has been suggested [S. Fauve, S. Douady, and O. Thaul, Phys. Rev. Lett. **65**, 385 (1990)] that an alternative description of the breaking of parity is to consider the order parameter as the difference between the phase of some harmonic of the pattern and that of the fundamental. Thus, in the case of the second harmonic, the pattern can be considered as the sum $U \simeq c_1 \cos[q_0(x+\phi_1)] + c_2 \cos[2q_0(x+\phi_2)]$. By defining $\Phi \equiv \phi_2 - \phi_1$, the pattern can be rewritten as $U \simeq c_1 \cos[q_0(x+\phi_1)] + \tilde{c}_2 c\,os[2q_0(x+\phi_1)] + c_3 \sin[2q_0(x+\phi_1)]$, where $\tilde{c}_2 = c_2 \cos(2q_0\Phi)$ and $c_3 = -c_2 \sin(2q_0\Phi)$. When viewed this way, a parametrization of the broken parity in terms of a phase mismatch is equivalent to the one proposed in Sec. II.

[18]See, e.g., *Solitons in Condensed Matter Physics,* edited by A. R. Bishop and T. Schneider (Springer, New York, 1978).

[19]P. Coullet and L. Gil (unpublished).

[20]See Ref. 17.

[21]K. Kawasaki and T. Ohta, Physica A (Amsterdam) **116**, 573 (1983); K. Kawasaki, Prog. Theor. Phys. Suppl. **79**, 161 (1984).

[22]J. Guckenheimer and P. Holmes, *Nonlinear Oscillations, Dynamical Systems and Bifurcations of Vector Fields* (Springer-Verlag, New York, 1983).

[23]L. Gil, Ph.D. thesis, Université de Nice, 1988.

[24]All numerical studies reported here were carried out by means of an implicit (Crank-Nicholson) algorithm, adapted from the standard version described in the literature to be applicable to coupled nonlinear equations of motion. See, for instance, W. H. Press, B. P. Flannery, S. A. Teukolsky, and W. T. Vetterling, *Numerical Recipes: The Art of Scientific Computing* (Cambridge Univesity Press, New York, 1986), Chap. 17.

[25]S. Koga and Y. Kuramoto, Prog. Theor. Phys. **63**, 106 (1980). See also G. B. Ermentrout, S. P. Hastings, and W. C. Troy, SIAM J. Appl. Math. **44**, 1133 (1984); T. Ohta, M. Mimura, and R. Kobayashi, Physica D **34**, 115 (1989).

[26]See also O. Thual and S. Fauve, J. Phys. (Paris) **49**, 1829 (1988); S. Leibler, V. Hakim, and R. E. Goldstein (unpublished).

[27]W. Eckhaus, *Studies in Non-Linear Stability Theory* (Springer-Verlag, New York, 1965).

[28]E. Abrahams and T. Tsuneto, Phys. Rev. **152**, 416 (1966); T. J. Rieger, D. J. Scalapino, and J. E. Mercereau, Phys. Rev. Lett. **27**, 1787 (1971), and references therein.

[29]T. J. Rieger, D. J. Scalapino, and J. E. Mercereau, Phys. Rev. B **6**, 1734 (1972), and references therein.

[30]B. D. Josephson, Phys. Lett. **1**, 251 (1962).

[31]A. Simon and A. Libchaber (private communication).

[32]Y. Couder, S. Michalland, and M. Rabaud (private communication).

[33]R. J. Watts-Tobin, Y. Krähenbühl, and L. Kramer, J. Low. Temp. Phys. **42**, 459 (1981).

[34]We are grateful to I. Procaccia (private communication) for important discussions related to the material of this section.

[35]See, e.g., A. K. Sen and D. E. Sullivan, Phys. Rev. A **35**, 1391 (1986), and references therein.

[36]P. G. de Gennes, Mol. Cryst. Liq. Cryst. **12**, 193 (1971).

[37]G. Goren, I. Procaccia, S. Rasenat, and V. Steinberg, Phys. Rev. Lett. **63**, 1237 (1989).
[38]J. Swift and P. C. Hohenberg, Phys. Rev. A **15**, 319 (1977).
[39]J. S. Langer, Acta Metall. **25**, 1121 (1977).
[40]See, e.g., C. Normand, Y. Pomeau, and M. G. Velarde, Rev. Mod. Phys. **49**, 581 (1977).
[41]For normal form analyses of the coupling of a fundamental mode and its second harmonic, see, G. Dangelmayr, Dyn. Stab. Syst. **1**, 159 (1986); D. Armbruster, J. Guckenheimer, and P. Holmes, Physica D **29**, 257 (1988), and references therein; M. R. E. Proctor and C. Jones, J. Fluid Mech. **188**, 301 (1988); R. E. Goldstein and V. Hakim (unpublished).
[42]See also Ref. 12.
[43]R. C. Brower, D. A. Kessler, J. Koplik, and H. Levine, Phys. Rev. Lett. **51**, 1111 (1983).
[44]E. Ben-Jacob, N. Goldenfeld, J. S. Langer, and G. Schön, Phys. Rev. A **29**, 330 (1984).
[45]B. A. Malomed and M. I. Tribelsky, Physica D **14**, 67 (1984).
[46]G. I. Sivashinsky, Acta Astronaut. **4**, 1177 (1977); Y. Kuramoto, Prog. Theor. Phys. Suppl. **64**, 346 (1978).
[47]G. I. Sivashinsky, Physica D **8**, 243 (1983); A. Novick-Cohen and G. I. Sivashinsky, *ibid.* **20**, 237 (1986); A. Novick-Cohen, *ibid.* **23**, 118 (1986).
[48]U. Frisch, Z. S. She, and O. Thaul, J. Fluid Mech. **168**, 221 (1986).
[49]See, e.g., J. M. Hyman and B. Nicolaenko, Physica D **18**, 113 (1986); B. I. Shraiman, Phys. Rev. Lett. **57**, 325 (1986).